Cement and Concrete Composites 148 (2024) 105466

Contents lists available at ScienceDirect

Cement and Concrete Composites

journal homepage: www.elsevier.com/locate/cemconcomp

Development of self-sensing ultra-high-performance concrete using hybrid carbon black and carbon nanofibers

Wengui Li [a,*], Yipu Guo [a,**], Xuanrui Zhang [a], Wenkui Dong [b], Xiaohu Li [c], Tao Yu [d], Kejin Wang [e]

[a] Centre for Infrastructure Engineering and Safety, School of Civil and Environmental Engineering, The University of New South Wales, NSW, 2052, Australia
[b] Institute of Construction Materials, Technische Universität Dresden, 01062, Dresden, Germany
[c] School of Infrastructure Engineering, Nanchang University, Jiangxi, 330031, China
[d] Department of Civil and Environmental Engineering, The Hong Kong Polytechnic University, Hong Kong, China
[e] Department of Civil, Construction and Environmental Engineering, Iowa State University, IA, 50011, USA

ARTICLE INFO

Keywords:
Ultra-high-performance concrete (UHPC)
Nanofillers
Conductivity
Piezoresistivity
Self-sensing
Equivalent circuit modelling

ABSTRACT

The self-sensing ultra-high-performance concrete (UHPC) was developed in this study by incorporating nano carbon black (CB) and carbon nanofiber (CNF) as additives into the UHPC matrix. Single CB and hybrid CB/CNF filled UHPCs were compared in terms of strength, microstructures, percolation threshold, conductivity, and piezoresistive sensing performance. The results indicate that hybrid CB/CNF filled UHPC consistently exhibits superior compressive strength compared to the counterpart with single CB. The percolation threshold begins at approximately 0.5 % CB content, regardless of the inclusion of CNF. The CNF serves to link the surrounding conductive passages contributed by CB nanoparticles, demonstrating the positive effect of hybrid nanofillers with multiple dimensions. AC impedance spectroscopy (ACIS) and equivalent circuit modelling were performed to understand the synergetic effect of CB/CNF on the electrical network in UHPC matrix and to compare the conductive characteristics between single CB and hybrid CB/CNF filled self-sensing UHPC. The insights gained from this analysis contribute to comprehending the conductive behaviours and sensing mechanisms at the microstructural level, providing new insight into the material design strategy to enhance the electrical and sensing performances of UHPC-based cementitious sensors. Regarding piezoresistive performance, the stability of sensing performance in response to dynamic cyclic load improves with an increasing content of conductive fillers; the hybrid fillers of CB/CNF enhance the stability of piezoresistive sensing performance of self-sensing UHPC with less signal noise under monotonic compressive loading. The outcomes can integrate the piezoresistive self-sensing capacity with UHPC to promote the application of cement-based sensors in civil infrastructure, offering potential benefits for structural health monitoring and maintenance.

1. Introduction

Cement-based composite is one of the most commonly used materials in global construction sector [1], owing to its superior performance-to-cost ratio, high durability, and easier adoptability. Nevertheless, various loading and environment actions, as well as natural and man-made disasters during the service life of the structures inevitably induce the cracks and flaws inside the composite, eventually leading to the catastrophic failure of the structures as due to the covalence of critical defects [2,3]. For critical components in structures, precise structural health monitoring is necessary to evaluate potential defects in cement-based composites and assess the health states of structures. This monitoring facilitates early warning systems, contributing to the extension of infrastructural longevity [4]. Over the past decades, various monitoring techniques such as optical fiber, piezo-ceramic, non-contact X-ray methods, and self-sensing cement--based or polymer-based sensors have been widely proposed [5]. In particular, the intrinsic self-sensing cement-based composite, referred to as cement-based sensors, have garnered increased attention recently. This is due to their advantages of low cost, high durability, adaptability, and automaticity [6,7].

On the basis of extensive efforts and numerous achievements in

* Corresponding author. Centre for Infrastructure Engineering and Safety, School of Civil and Environmental Engineering, The University of New South Wales, NSW, 2052, Australia.
** Corresponding author.
E-mail addresses: wengui.li@unsw.edu.au (W. Li), yipu.guo-1@uts.edu.au (Y. Guo).

https://doi.org/10.1016/j.cemconcomp.2024.105466
Received 29 July 2023; Received in revised form 2 January 2024; Accepted 31 January 2024
Available online 1 February 2024

developing cement-based sensors with a normal strength cement matrix, researchers are now shifting their focus toward UHPC-based sensors [8]. However, existing research on the electrical and piezoresistive behaviors of UHPC-based sensors is relatively limited. UHPC is gaining increased attention due to its superior mechanical and durability performance compared to normal strength composites. The outstanding durability of UHPC, achieved through refined porosity and improved impenetrability, makes it nearly impervious to erosion by harmful substances or deterioration [9]. The development of UHPC is typically realized by reducing water-to-binder (w/b) ratio, optimizing particle packing density, and processing special curing method [10]. The piezoresistive sensing property of cement-based sensors is induced by its tailored electrical conductivity, requiring the introduction of electrically conductive carbonic or metallic fillers. Among various conductive fillers, carbon nanomaterials such as carbon nanotubes (CNT), carbon nanofibers (CNF), and graphene nanoplatelets (GNP) are predominantly preferred as electrically conductive fillers due to their effectiveness at very low content (high aspect ratio) and their nano-reinforcing effect [11,12].

Seo et al. [11] conducted a systematic evaluation of the physico-chemical properties, autogenous shrinkage, hydration kinetics and products, mechanical properties, and piezoresistive sensing properties of UHPC filled with 0.1–0.5 % thin-walled CNTs. The results indicated an electrical percolation threshold of approximately 0.2 % the highest piezoresistive sensitivity in response to cyclic compressive loading. Moreover, specimens filled with more than 0.2 % CNTs exhibited a more stable sensing response regardless of the loading magnitude and frequency. Further, Jung et al. [13] investigated the electrical curing efficiency and crack sensing capability of UHPC sensor filled with CNT and steel fibre. It was confirmed that electrically cured samples possessed more favourable deflection harden and multiple cracking properties subjected to flexural stress. Guo et al. [14] explored the pore structure and stress sensing properties of silane-treated GNP. Refined porosity about 11.5 % with least harmful pores and highest piezoresistive sensitivity were found in UHPC with 0.05 % GNP. Wang et al. [15] compared the sensing performance of incorporating Carbon Nanofibers (CNF) into different cement matrices, including reactive powder concrete, cement paste, and mortar. Better sensing performance with higher sensitivity and linearity was demonstrated in CNFs-filled reactive powder concrete. The proper inclusion of carbon nanomaterials can modify matrix packing and reduce shrinkage and porosity, simultaneously securing the inherent characteristics of electrical conductivity and superior mechanical properties, pertaining to carbon nanomaterials and UHPC, respectively. Thus, the development of carbon nanomaterials filled UHPC with intrinsic self-sensing property is a promising approach.

Compared with one-dimension (1D) or two-dimensions (2D) carbon nanomaterials (i.e., CNT, CNF, and GNP), zero-dimension (0D) nano-carbon black (CB) is rarely explored as conductive fillers to manufacture UHPC-based sensor because of its inferior effectiveness in tailing the conductivity, mechanical properties, and self-sensing capacity. Nevertheless, many favourable advantages involving low cost, relative ease of dispersion, and high thermal and chemical stability, make it increasingly attractive. To address the disadvantages of single CB filled cement-based sensors, many studies proposed hybrid incorporation of CB with another fibrous nano or micro sized conductive fillers such as carbon fibre (CF), CNT, nickel nanofiber (NiNF) to endow the positive synergic effect [16–18]. CB particles play the role of a short-range conductor, while the other fibrous conductive filler functions as a long-range conductor, stimulating the formation of rich conductive paths [19]. Stable and sensitive piezoresistive behaviours were achieved in cement-based sensors with hybrid CB/CNT fillers in response to cyclic compressive loading [17] and monotonic compressive loading [20]. Further, Ding et al. [21] embedded hybrid CB/CNT small-scale cement-based sensor into large-scale concrete column and Liang et al. [22] applied CB/CNT hybrid fillers into glass fiber reinforced polymer reinforced concrete beam, the sensing signal from cement-based sensors can be precisely correlated to the stress and deformation states of the concrete column/beam. The above studies verified excellent self-sensing properties for hybrid inclusion of CB with another fibrous conductive filler to achieve the favourable synergistic effect in cement-based sensors made with normal strength cement matrices. To the best of our knowledge, there is a lack of study on the development of hybrid CB/CNF filled UHPC and its piezoresistive sensing capacity. To date, no research has been conducted to compare the conductive and self-sensing behaviours between single CB and hybrid CB/CNF filled self-sensing UHPC. More importantly, although the above studies agreed that the hybrid use of conductive fillers contributed to the favourable synergistic/composite effect, they mainly captured such synergistic effect based on SEM graph observation or deduced from resistivity results. The former only reflects the localized area and the latter lacks the experimental evidence, which somehow lacks reliability. In this sense, the exact features, and mechanisms relevant to how hybrid conductive systems comprised by multi-phase, multi-scale, and multi-dimension functional contribute to the continuity of conductive network (i.e., whether electrical percolation or not and how fibrous functional filler take advantage of their fibrous shape and high aspect ratio) is still unclear and merely explored.

To this context, the single CB filler and hybrid CB/CNF fillers with fixed dosage of fibrous CNF were employed to prepare the smart UHPC with intrinsic self-sensing capacity. Firstly, material characterizations of strength, phase composition, and microstructures were conducted by using compressive test, X-ray diffractometry (XRD), scanning electron microscopy (SEM) and energy dispersive X-ray spectrometry (EDX). The conductivity was measured by direct current (DC) four-electrode method and the percolation threshold was determined. Alternative current (AC) impedance spectroscopy (ACIS) and equivalent circuit modelling were performed to understand the synergetic effect of CB/CNF on the electrical microstructure in UHPC matrix and compare the conductive characteristic between single CB and hybrid CB/CNF filled smart UHPC. A relevant analysis of the variations in equivalent circuit element is beneficial for extracting essential details and validating the proposed equivalent circuit model. Finally, the piezoresistive sensing performances of two types of UHPC were comprehensively assessed by three compressive loading protocols including quasi-static cyclic load, dynamic cyclic load, and monotonic compressive load [23,24].

Table 1
Main physical and chemical properties of nanocarbon black (CB).

Average particle size (nm)	Resistivity (Ω·cm)	Compacted density (g/l)	DBP (ml/100g)	Surface area (m^2/g)	pH	Ash content (%)
30–45	<0.43	280–300	280	120–130	7.5	<0.3

Table 2
Main physical and chemical properties of carbon nanofiber (CNF).

Colour	Specific area (m^2/g)	Diameter (nm)	Length (μm)	Purity (%)	Metal content
Black	15–30	50–200	5–15	>99.9 %	<100 ppm

2. Experimental program

2.1. Materials and preparation

Commercially available General Purpose (GP) cement and silica fume, which are confirmed to AS3972 and AS3583 respectively, are served as binder material. The Main physical and chemical properties of CB and CNF are presented in Tables 1 and 2, respectively. The mix design for both single CB filled, and hybrid CB/CNF filled UHPC is shown in Table 3, which is customized based on UHPC mix previously designed in Ref. [10]. Fine grade micro silica sand (ACI Dry Sand Holusil

Table 3
Mix design of CB/CNF filled cement-based sensor.

Group	Cement	Silica fume	Silica sand	Water	CB (%)	CNF (%)	Superplasticizer (%)	Defoamer (%)
Plain	0.89	0.11	0.4	0.22*	0	0	1.0	0.13
Single CB filled samples								
05CB	0.89	0.11	0.4	0.22	1.0	0	1.3	0.13
10CB	0.89	0.11	0.4	0.22	0.5	0	1.1	0.13
10CB	0.89	0.11	0.4	0.22	1.0	0	1.3	0.13
Hybrid CB/CNF filled sample								
05CB02CNF	0.89	0.11	0.4	0.22	0.5	0.2	1.6	0.13
10CB02CNF	0.89	0.11	0.4	0.22	1.0	0.2	1.8	0.13
20CB02CNF	0.89	0.11	0.4	0.22	2.0	0.2	2.0	0.13

Note: number under the cement, silica fume, CB, water, superplasticizer and defoamer represent their ratios to the weight of binder, e.g., 0.22* under water means the water to binder ratio of 0.22.

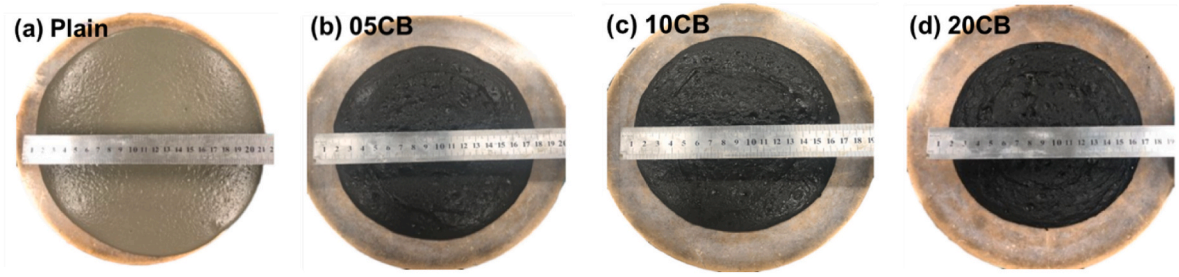

Fig. 1. Table flow diameters of plain and mono CB filled UHPC samples.

4005 Kiln Dried Sand) was used, which contains crystalline silica proportion >98 % with the average particle size of 150 μ m. The UHPC matrix has a water-to-binder ratio of 0.22 and sand to binder ratio of 0.4. The dosage of Polycarboxylic-based high range reducer (Sika VescoCrete-140 SK) positively matched single or hybrid nanofillers amount from 1.0 % to 2.0 % to assure the adequate workability and proper dispersion of nanofillers. Defoamer (silicon emulsion with <5 % phosphates) is used to mitigate the air entraining effect. The doping dosage of superplasticizer positively matching the increased CB/CNF content to assist the dispersion of CB nanoparticles and ensure the similar workability of single CB filled and hybrid CB/CNF filled UHPC samples. The table flow diameter tested in accordance with ASTM C1437-20 [25] is around 220 mm for plain sample and 180 ± 10 mm for single CB filled and hybrid CB/CNF filled samples shown in Fig. 1

The specimen manufacturing process is described as follow. The first step is to prepare CB/CNF added superplasticizer/water solution (CB/CNF suspension). The pre-determined amount of CB/CNF is added into the beaker with a weight mixture of water and superplasticizer, followed by gentle stirring and ultrasonic dispersion. To enable the optimized dispersing efficiency, the ultrasonic treatment with a frequency of 40 Hz was combined with high-speed stirring of 2000 rpm and lasted for 40 min. The water bath was updated every 10 min to prevent the potential negative impact on the dispersion efficiency of CB/CNF nanoparticles that potentially raised by elevated temperature. Cement, silica fume and silica sand were dried mixed in Hobart mixer for 5 min. After that, half amount of mixture of ultrasonicated CB/CNF suspension and the deformer were poured into mixture and mixed for 3–4 min, then the remaining half of ultrasonicated CB/CNF suspension were generally poured into the fresh slurry for another 3–4 min. The fresh mixture was casted into the 50 mm × 50 mm × 50 mm cubic mould. Four electrodes were embedded during the casting of the specimens. The width and embedment length of the electrodes are 25 mm and 35 mm. The specimens were initially cured 2 days in standard curing chamber with 25 °C temperature and 95 % relative humidity before being demoulded and then were steam-cured with the temperature maintained at 90 °C for additional 3 days. After that, the samples were moved again into the standard curing chamber until 28 days. Prior to the electrical and piezoresistive measurements, the specimens were dried in 60° oven for 24 h. Fig. 2 schematically plots the manufacturing process of single CB filled UHPC and hybrid CB/CNF filled UHPC samples.

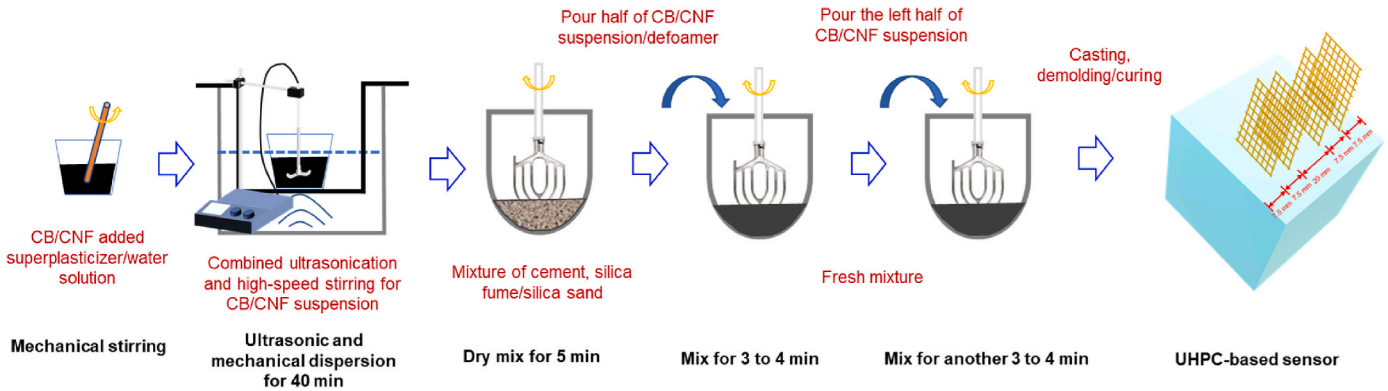

Fig. 2. Preparation procedures and specimen of CB/CNF UHPC-based sensors.

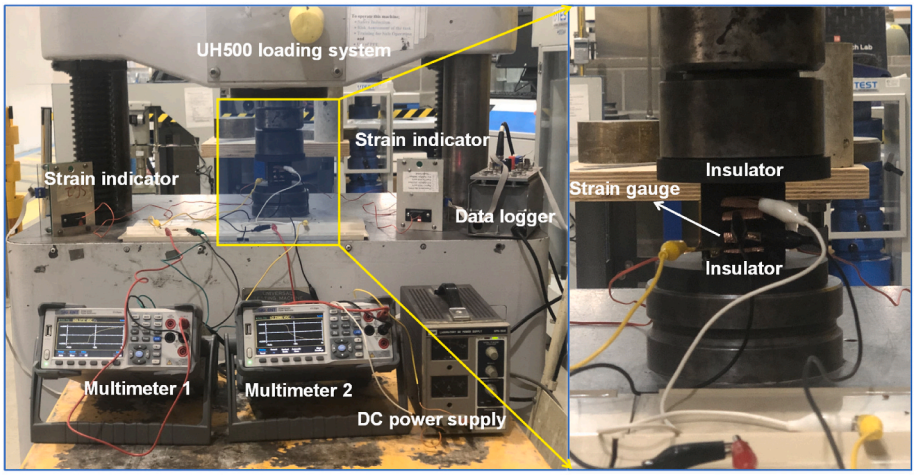

Fig. 3. Test setup of the piezoresistivity experiments.

2.2. Experimental methods

Sample powders for X-ray diffraction (XRD) were acquired by sieve passing apertures of 75 μ m. XRD test was conducted by a BRUKER AXS D8 ADVANCE machine with 40 kV power and 40 mA. The scanned Cu-Kα range was 5 °- 70 ° 2 θ (°) and the step is 0.018 °/S. Compressive strength tests were performed on 50 mm × 50 mm × 50 mm cube specimens using the equipment SHIMADZU UH500 with a loading rate of 0.5 mm/min 3 replicates were tested for each group. Field mission scanning electron microscopy (SEM, Zeiss Supra 55VP) coupled with energy dispersive X-ray spectrometry (EDX) was used to investigate the microstructures and distribution of conductive phases in single CB filled and hybrid CB/CNF filled UHPC samples. Small and flat pieces were collected from the inner core of fractured specimens. The four-probe DC method is used to measure the static electrical conductivity. The specific configuration is identical to the authors' previous study [26]. The DC electrical resistivity (ρ_{dc}) of the sample can be calculated by Eqs. (1) and (2):

$$R_s = \frac{U_s}{I_s} = \frac{U_s}{\frac{U_r}{R_r}} = \frac{U_s R_r}{U_r} \tag{1}$$

$$\rho_{dc} = \rho_s = \frac{R_s A}{L} = \frac{U_s R_r A}{U_r} \tag{2}$$

where ρ_s and R_s are the electrical resistivity and resistance of sample in Ω • cm and Ω, respectively; U_s and R_s denote the voltage and current of the sample; U_r and R_r denote the voltage and resistance of resistor; A is the cross-section area of electrodes embedded into the sample; L is the resistance between inner two electrodes.

The AC impedance spectroscopy (ACIS) is performed by Solartron SI 1260 frequency response analyser (RFA). Two-probe method was applied on inner two electrodes of the samples during the ACIS test [27], considering the popularity and reliability of two-probe measurement method [28]. The specific arrangement of two-probe configuration between 1260 RFA and the sample is detailed in Ref. [29]. To obtain the ACIS, the AC frequency charged in the range of 1 Hz–10 MHz with a potential amplitude of 250 mV versus the open circuit potential. The ACIS results were analysed according to equivalent circuit method using ZView software.

The resistivity was recorded using a 4-probe method during the piezoresistivity tests. The test setup is illustrated in Fig. 3. Two strain gauges were attached on both sides of the specimens. Two Teflon plates was put at both upside and bottom sides of the samples to electrically isolate samples from loading plates. The compressive loading was performed by SHIMADZU UH500 loading system. Three different loading regimes including: 1) quasi-static cyclic loading; 2) dynamic cyclic loading; and 3) monotonic compressive loading until failure were applied to thoroughly evaluate the piezoresistive self-sensing performance of single CB filled and CB/CNF filled UHPC samples. Quasi-static cyclic loading regime consists of two stress magnitudes of 20 MPa and 40 MPa with the loading rates of 2.5 kN/s and 5 kN/s, respectively. Four loading-unloading cycles were applied for each stress magnitude. The dynamic cyclic loading regime consists constant stress magnitude of 20 MPa and varied six frequencies 0.1, 0.2, 0.3, 0.5, 0.9 and 1.6 Hz, based on logarithmic sampling method ($lgf(n) = lg\,0.1 + n(lg\,5 - lg\,0.1)/7, n = 1, 2, \ldots.5$), which is consistent with the typical frequency of dynamic response in large civil engineering structures [30,31]. As for the monotonic compressive loading regime, the loading rate was kept at 1.5 kN/s. For the quasi-static cyclic loading and monotonic compressive loading, the data sampling rate was 5 Hz. For the dynamic cyclic loading, the data sampling rate is 50 Hz. For all piezoresisvity tests, the samples were electrified 10 min before the tests to eliminate the polarization effect due to DC source. During the compressive loadings, the electrical resistivity was recorded. The fractional change in resistivity (FCR) is defined as Eq. (3):

$$FCR = \frac{\rho - \rho_0}{\rho_0} \tag{3}$$

where ρ_0 is the initial static resistivity, ρ is the real-time resistivity of the samples during the loading.

The stress sensitivity (SS) and gauge factor (GF) are two significant parameters to evaluate the piezoresistive sensing sensitivity, which can be calculated by Eqs. (4) and (5):

$$SS = \frac{FCR}{\sigma} \tag{4}$$

$$GF = \frac{FCR}{\varepsilon} \tag{5}$$

Linearity error (LR) is proposed to evaluate piezoresistive sensing performance in terms of linear response, which is based on Eq. (6).

$$LR = \frac{\Delta Max}{FCR_f} \times 100\% \tag{6}$$

where ΔMax denotes the maximum deviation between piezoresistive and linear fitting line; FCR_f denotes the full-scale output of FCR. A large linearity error refers to a reduced linearity degree of the piezoresistive response.

Signal to noise ratio (SNR) is an important parameter to assess the piezoresistive sensing stability. SNR refers to the ratio between signal

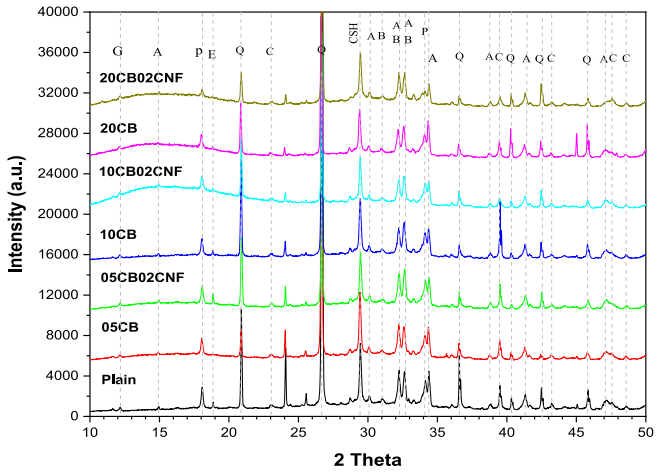

Fig. 4. XRD patterns of the all groups (A: alite; B: belite; C: calcite; E: ettringite; G: gypsum P: portlandite; Q: quartz; C–S–H: calcium silicate hydrate.).

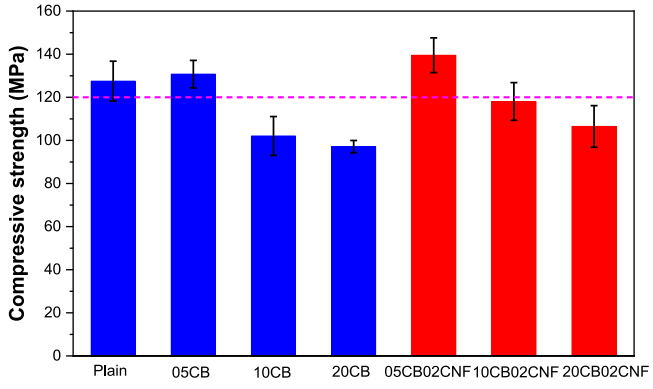

Fig. 5. Compressive strength of UHPC filled with CB or hybrid CB and CNF.

and noise. The unit of SNR is dB, and a larger SNR value represents an enhanced piezoresistive sensing performance with less noise signal. The formula of SNR is defined in Eq. (7).

$$SNR = 10\ log_{10}\left(\frac{P_s}{P_n}\right) = 10\ log_{10}\left(\frac{A_s^2}{A_n^2}\right) \tag{7}$$

where P_s and P_n denote the power of signal and noise, respectively. A_s and A_n denote the amplitude of signal and noise, respectively.

3. Result and discussion

3.1. X-ray diffusion

The XRD patterns of all groups are illustrated in Fig. 4, and the remarkable peaks corresponding to the quartz are associated with the presence of silica sand. The peaks of unhydrated cement clinkers such as alite, belite and gypsum can be captured. Overall, the peaks located in seven groups are similar because of the inert nature of CB and CNF [32,33], implying there is no newly generated phases. Both CB and CNF act as inert filler in the UHPC matrix, which not alter the chemical structure of the hydrated cement products. The weak ettringite peak is captured since the it is thermally decomposed during the heat curing [34]. There are some peaks corresponding to calcite is stemmed from inevitable carbonization during the sample preparation [33]. The Intensities of peaks at ($2\theta = 18^\circ$ and 28°) corresponding to portlandite (CH) are decreased for single CB filled and hybrid CB/CNF filled samples compared to plain ones. The intensities of hybrid CB/CNF filled samples are smaller single CB filled ones. With the presence of silica fume, the portlandite was partially consumed to form C–S–H owing to pozzolanic reaction [11]. Although a qualitative comparison of the degree of hydration (DOH) among the groups is hard in the case of XRD patterns [34], The intensity of CH is gradually decreased with increasing CB content, suggesting that extensive CB content hinder the cement hydration. In particular, the intensity of CH is distinctively lower for 20CB20CNF compared to the other groups, indicating that excessive conductive fillers pose a negative effect on cements hydration, which is consistent with the previous studies [32,35].

3.2. Mechanical strength

The compressive strengths of all groups are shown in Fig. 5. For both single CB and hybrid CB/CNF filled samples, the compressive strengths slightly increase when CB content is 0.5 % and then remarkably decrease when CB contents reach the 1.0 % and 2.0 %. Such variation trend is consistent with literature of CB filled cement composite with various CB contents [32,35,36]. The initial increase of compressive strength is mainly attributed to the filling effect of CB and reduction effect of harmful pores, considering quantitative results of previous study [32]. A proper amount of nanoscale CB particles modify the particles size distribution and densify the cement matrix [36]. The remarkably reduced compressive strength is mainly ascribed to the absorption of free water, CB agglomerations, and superplasticizer, which pose a downside influence on cement hydration and fluidity, thus affecting the particle size distribution and compressive strength [37]. In addition, studies proposed CB is detrimental to the binding strength among the hydration products [32]. Moreover, the reduced compressive strength is probably owing to the dilution effect where the reduced cement content impedes the development of strength [35].

The remarkable decrease in compressive strength might also be partially interpreted by the deteriorated microstructures of the specimens. The microstructures of 05CB02CNF and 20CB02NCF are illustrated in Figs. 6 and 7, respectively. It is detected 05CB02CNF shows a relatively compact microstructure compared to 20CB02CNF with less microdefects. Some micropores and cracks can be detected in 20CB02CNF. Fig. 6 (a) shows the CB and CNF are tightly embedded in the cement matrix in 05CB02CNF. The needle-like objectives shown in Fig. 6 (d), which should be a bundle of ettringites and CNFs [38], are tightly bonded with hydrate phases, demonstrating a improved and compact microstructure. Differently, characteristic microstructures with increased porosity and nonuniformity can be detected for 20CB02CNF shown in Fig. 7. Fig. 7 (a) shows the local defects near the ITZ surrounding the sand grain. Abundant and incompact CB/hydration products aggregates in the ranges of hundreds of nanometres to 1 μm can be detected, showing relatively porous microstructure. Fig. 7 (d) shows the CB agglomerations typically in several hundred nanometres, which become the defects and stress concentration points in the cement matrix with weak bearing capacity to external loading [2,39]. The distinctively microstructural characteristics between 05CB02CNF and 20CB02CNF reveal that a proper amount of CB can possess a positive effect on porosity and microstructure, while excessive amount of CB can easily form the CB agglomerations and possess downside effect on porosity and microstructure.

In terms of effect of CNF, it is seen that hybrid CB/CNF filled samples always show the superior compressive strength than single CB filled samples, regardless of the CB content. As revealed in Figs. 6 and 7, the bundled CNF cannot be found from both samples but the individual CNFs that are well anchored in the hydration product. Previous studies [40,41] confirmed that incorporating a proper amount of well-dispersed CNF could yielded a significance increase of compressive strength of the cement composites. The bridging effect of CNFs can be found in Fig. 7 (c). There is a layer of Ca–Si rich phase tightly bonded to the surface of

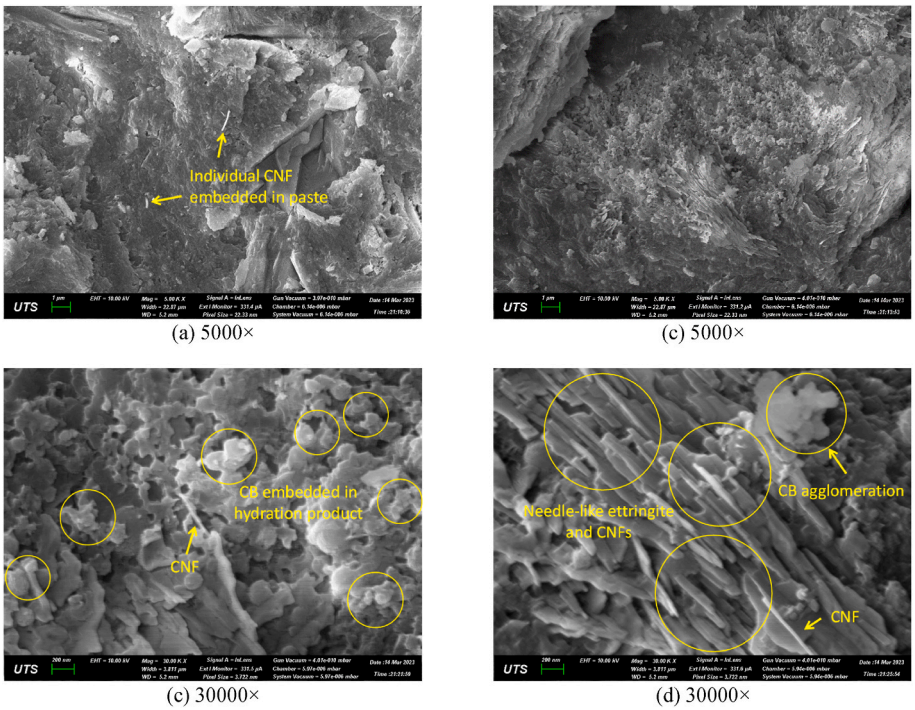

Fig. 6. Microstructures of UHPC with 0.5 % CB and 0.2 % CNF (05CB02CNF).

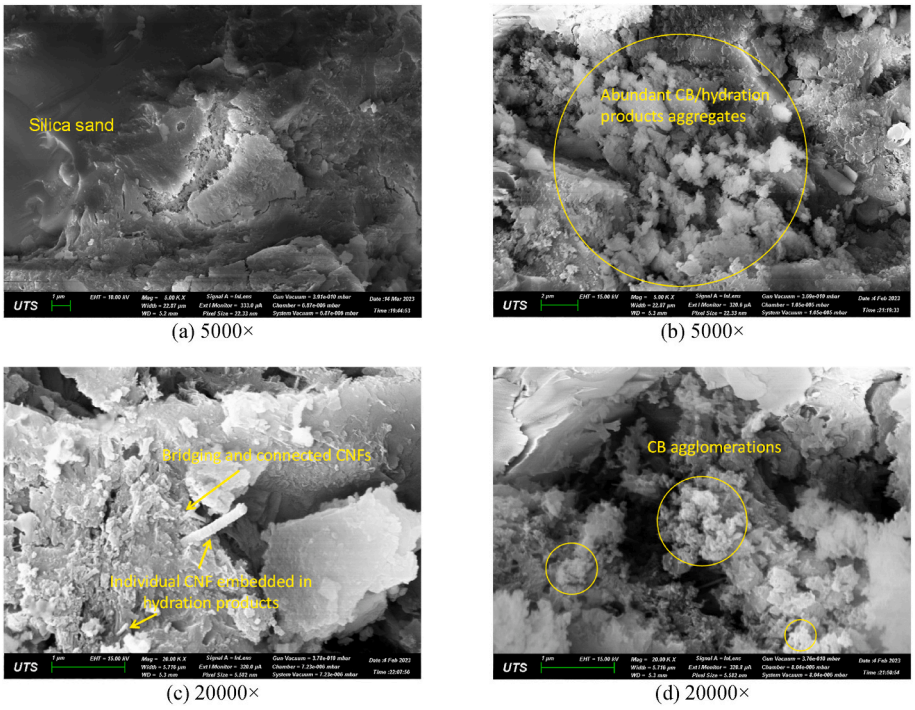

Fig. 7. Microstructures of UHPC with 2.0 % CB and 0.2 % CNF (20CB02CNF).

CNFs, which can be captured in the following Fig. 9. With the presence of silica fume particles, the dispersed CNF provides potential nucleating sites for the self-assembly of Ca–Si rich phases, which is possibly attributed to the abundant exposed edge planes along the CNF surface [42]. In addition, the presence of silica fume particles can promote the progressive generation of Ca–Si phase either encircle the CNFs or in the interstices of CNF network through the decrease of effective hydrophobicity, enabling the disposition of Ca–Si rich phases and CH and a more pronounced embedment of CNFs in the hydration products [42] in Fig. 7 (e). These positive interactions between CNF and cement phases should explain the improved hybrid CB/CNF filled samples compared to single CB filled samples regardless of CB dosages observed in the current study. Nevertheless, not all groups fulfill the definitive requirement of UHPC of 120 MPa according to C1856/C1856M − 17 [43], the mix design should be further optimized for future research.

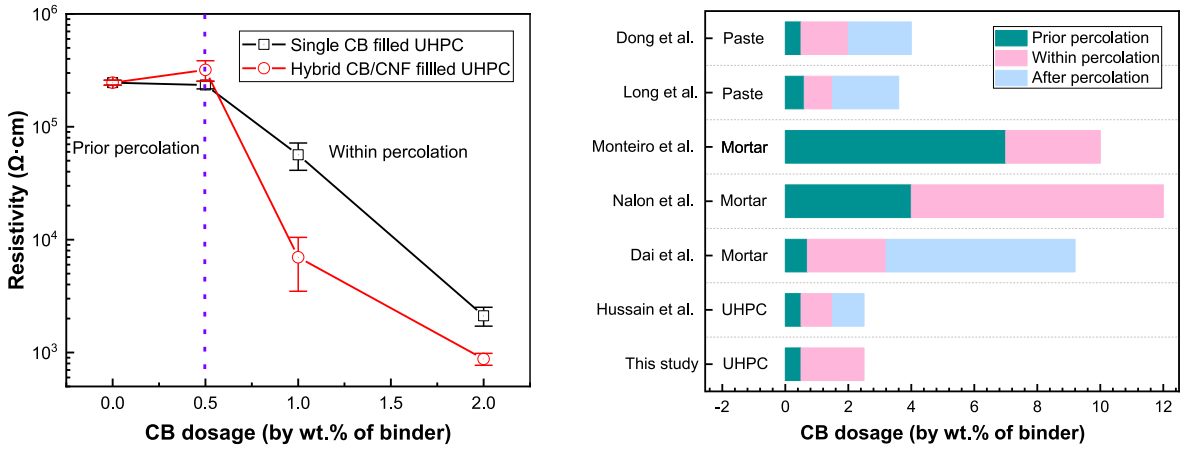

(a) Percolation zone (b) Comparative analysis

Fig. 8. Percolation zone of single and hybrid filled UHPC specimen and comparison with other studies [36,45,46,50–52].

3.3. Electrical conductivity

Fig. 8 (a) shows the resistivity of single CB and hybrid CB/CNF filled samples as a function of CB dosages. Fig. 8 (b) summarizes the percolation thresholds for single CB filled cement composites from previously reported articles. Some studies reported a distinctively high percolation zone. The discrepancy is mainly stemmed from the different structural properties of CB particles such as size and dibutyl phthalate (DBP) given that there are many types of CB commercially available. CB particles with smaller size (higher specific area) and higher DBP absorption (large number of CB nanoparticles made for the primary aggregate), as so-called higher structure, often contributes to lower percolation thresholds [44,45]. In addition, the presence of fine and coarse aggregates is another factor to determine the percolation zone [5]. Nevertheless, it is seen that most studies reported a starting percolation threshold of in the range of approximately 0.5–0.7 %, which validate the results observed in present study. In the case of hybrid CB/CNF filled UHPC, although similar percolation trend is shown, the inclusion of 0.2 % CNF as additive nanofillers significantly reduces the resistivity of single CB filled UHPC, with nearly one order and two thirds, respectively for the cases of 1.0 % CB and 2.0 % CB. It is noted there is an increase of resistivity for the case of 0.5 % CB. The increase of resistivity is likely due to the combination effect of additional inclusion of superplasticizer [46] and more compact matrix [47]. The superplasticizer will alter the microstructural and interfacial characteristics of silica sand mortar, resulting in that superplasticized mortars always presents the higher electrical resistivity compared to the control samples [48,49]. Overall, the significantly reduced resistivity evidences the positive synergistic effects of the hybrid use of nanofillers with different size and dimensions.

Fig. 9 illustrates how CNFs take the advantage of their fibrous shape and high aspect ratio in improving the length and continuity of the conductive passages. Previous studies illustrated that spherical CB nanoparticles are embedded with the hydrated products and as seeding for C–S–H nucleating on, therefore CB nanoparticles distributed in the cement matrix in the integrated form of hydrated products due to hydration and pozzolanic reactions of cementitious materials. Fig. 9 (a) shows the single CNF embedded in the compact cementitious matrix of 05CB02CNF. EDS mapping spectrum clearly demonstrates that role of CNF links the surrounding conductive passages contributed by CB nanoparticles, evidencing the cooperative modification effect brought by the hybrid usage of nano additives with different sizes and dimensions. The fibrous CNF with larger diameters function as conductive carrier and link the CB at long distance. Point spectrums 1 and 3 on CNF surface imply there are two distinctive types of CNF. Point spectrum 1 with high atomic ratio of carbon element suggests that the CNF is marginally wrapped by hydrated products, whereas spectrum 3 with less carbon intensity should correspond to the CNF that is broadly wrapped by hydrated products [38,41]. Point spectrum 2 is related to CB embedded in cement matrix.

More detailed characteristics of the latter type of CNF can be captured in 20CB02CNF as shown in Fig. 9 (b). It is seen that rich hydration products are tightly bonded on the certain part of the CNF surface zone as confirmed by point spectrums. The tight bonding between CNF and surrounding CB/hydration products in UHPC samples should be beneficial to the formation of continuous passages since localized defects can block the conductive passages [53]. One evidence is that the resistivity drop range is much higher than the resistivity drop results previously reported who compared hybrid use of CB and nickel nanofiber (NiNF) with single use of CB in cement paste samples, even with less content of CNF compared to NiNF [18]. In addition, the botryoidal chain structure of CB particles deposited on CNF surface can be clearly observed in Fig. 9 (b), implying the efficiency of CNF in establishing the rich conductive passages. In contrast to the mapping spectrum of 05CB02NCF, the CNF cannot be differentiated from the surrounding matrix by the intensity of carbon elemental map for 20CB02CNF shown in Fig. 9 (b). This is attributed to the high dosage of 2.0 % CB and the fact the CNFs are broadly bonded/wrapped by CB/hydration products, which should explain the different resistivity changes for the samples with various dosages of CB when adding the 0.2 % CNF. As shown in elemental maps in Fig. 9 (a), when CB content approaches the start of the percolation zone (i.e., 0.5 %), the CB particles are marginally distributed in the matrix. Although CNF can efficiently link the neighbouring CB communities as presented, such cases should be considered as localized situation. For the highest CB content of 2.0 %, the linkage effect of CNF on promoting the conductive passages also compensate to certain degree because of already percolated conductive network. Therefore, the maximum extent of drop in resistivity happens in intermediate CB content of 1.0 %. In addition, the Ca/Si ratios from all points spectrums on CNF surface are generally between 1.2 and 2.3, which is defined as typical C–S–H gel [41,54], implying rich C–S–H in the bonding between CNF and the matrix. However, previous studies proposed that rich CH crystals and perhaps C–S–H were nucleated on the surface of steel fibre in hybrid CNT/steel fibre filled UHPC [55,56]. Since rich C–S–H gel have a stronger bonding effects than CH crystals [57], better bonding promotes the CB to be tightly bonded to CNF surface. This phenomenon might reveal the advantage of using hybrid conductive fillers at nano scales compared to the counterparts at nano and micro/macro scales, in terms of both mechanical and electrical enhancements.

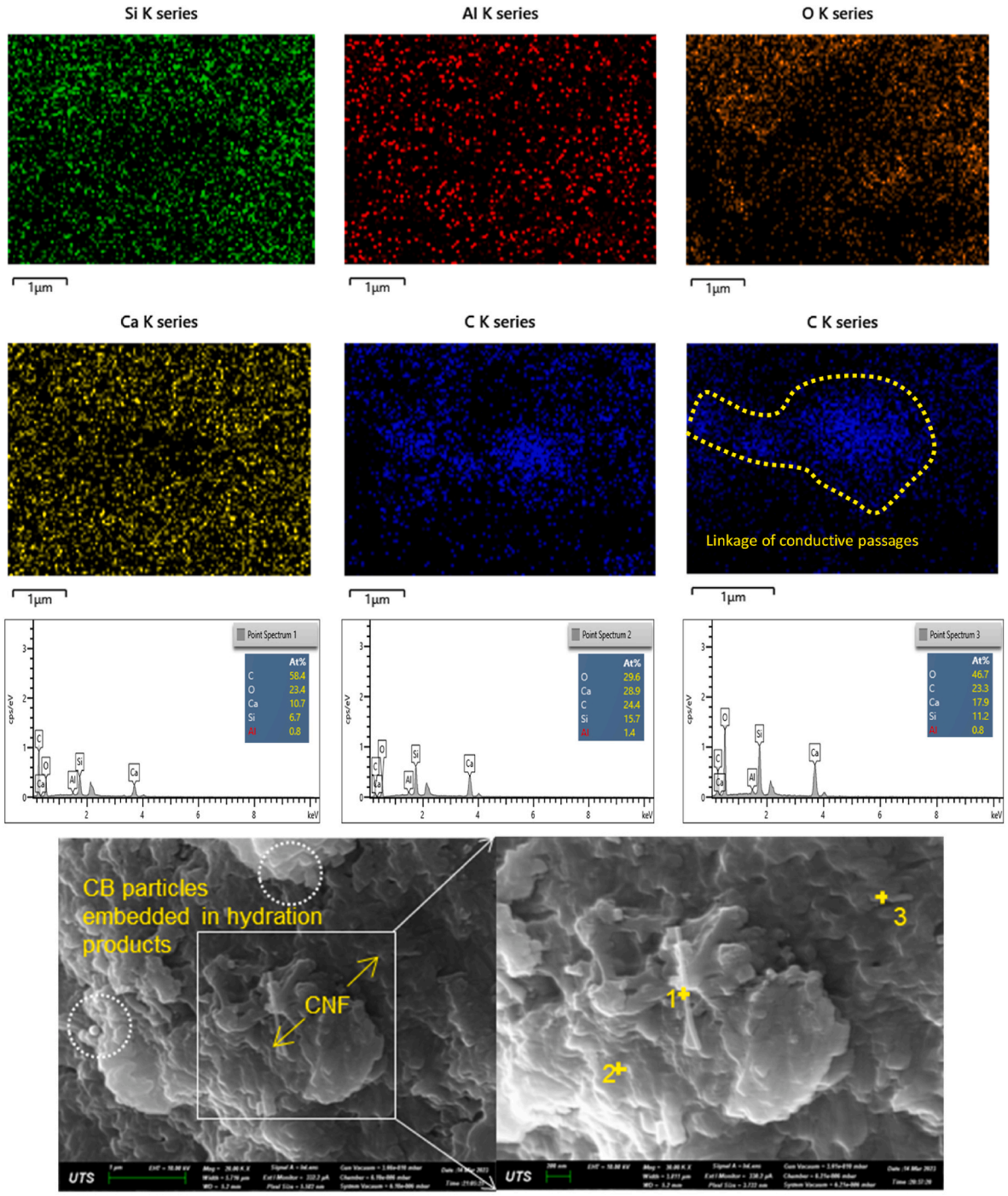

(a) 05CB02CNF

Fig. 9. Morphologies of 05CB02CNF and 20CB02CNF.

3.4. Analysis on equivalent circuit model and ACIS

3.4.1. AC impedance spectrum response

The AC impedance spectrum (ACIS) describes the frequency dependence of the impedance for composite materials, which is usually presented by Nyquist plots (Imaginary part vs Real part) [58]. The plots are parameterized in terms of frequency and usually involve a succession of semicircles that are associated with electrochemical response of the individual material components [59]. The partial convolution feature between different arcs is attributed to the similar relaxation times of multiple involved responses [60]. According to the literature [61–63], the typical Nyquist plot for plain cementitious composite include a single high frequency semicircle and an low frequency arc corresponding to the effect of external electrode, whereas the cementitious composite with the inclusion of conductive fillers presents two separated semicircles in addition to electrode arc. The origin of dual semicircles characteristic was explained by a "frequency-switchable coating model" in some studies on carbon fibre reinforced composites [63]. The schematic diagram for typical Nyquist plots for plain UHPC and UHPC containing conductive fillers are shown in Fig. 10 (a). For the case of

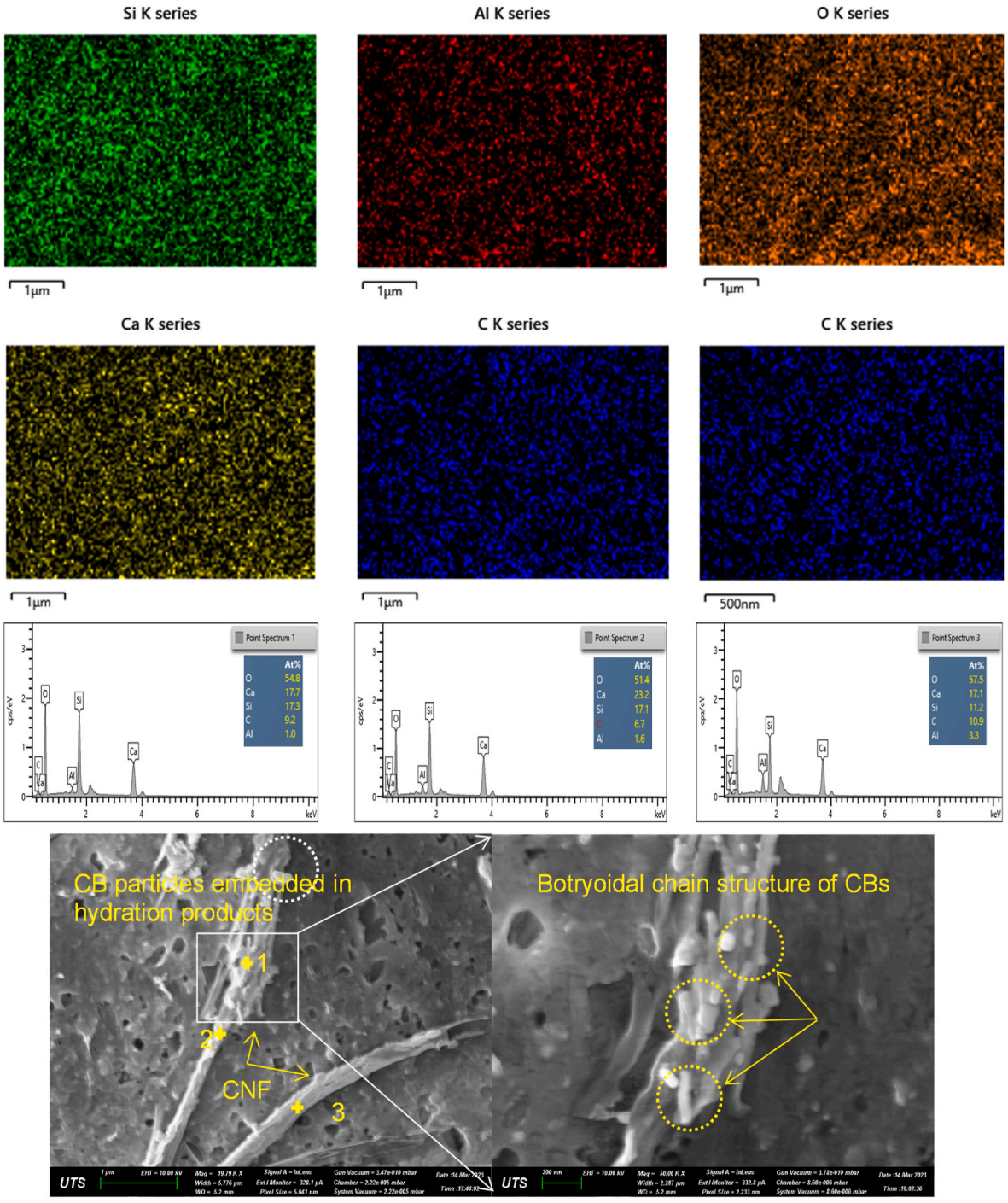

(b) 20CB02CNF

Fig. 9. (*continued*).

UHPC containing conductive materials, the left-side R_{cusp} is directly as result of short circuit of conductive materials and accounts for the combined transfer of electron current through the conductive materials and ionic current through the electrolyte [60], whereas right side R_{cusp} was attributed to AC resistance of the cement matrix and coincided with the four point DC resistance of composite [63–65]. Fig. 10 (b) compares the R_{cusp} values extracted from ACIS with R_{DC} values measured from four point method [60]. It is indicated that right-side R_{cusp} generally coincides with the R_{DC}, which supports the percolation zone analysis in the previous section. In addition, the left-side R_{cusp} for UHPC containing conductive fillers is relatively smaller than right-side R_{cusp}/R_{DC} with the increase of CB/CNF content, and it gradually becomes almost coincide when the CB/CNF content enters the percolation zone, in which the number and continuity of conductive passages greatly improved (i.e., for the cases of 10CB02CNF, 10CB and 20CB02NF). This phenomenon should further substantiate the fact that left side R_{cusp} is as a direct consequence of short-circuit of conductive materials. Therefore, the relationship between left-side R_{cusp} and right-side R_{cusp}/R_{DC} can be potentially used to identify the conductive states inside the cementitious composites. In addition, the impedance spectrums of 10CB02CNF and 20CB02CNF remarkably shift from higher value to smaller value along real axis by an order of magnitude compared to the counterparts of 10CB

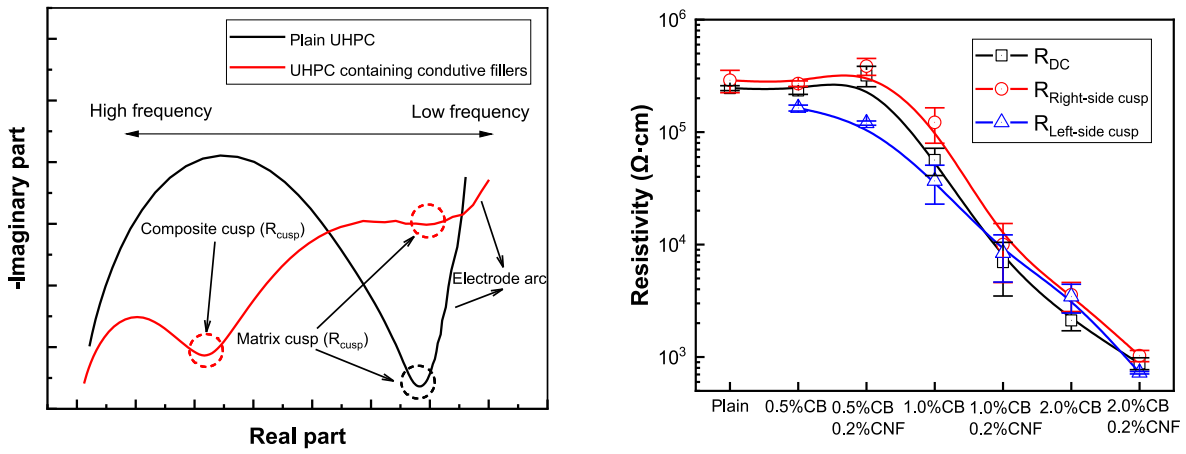

(a) Typical Nyquist plots (b) R_{DC}, left-side R_{cusp} and right-side R_{cusp}

Fig. 10. Typical Nyquist plots for plain UHPC and UHPC containing conductive fillers and comparisons of R_{DC}, left-side R_{cusp} and right-side R_{cusp}.

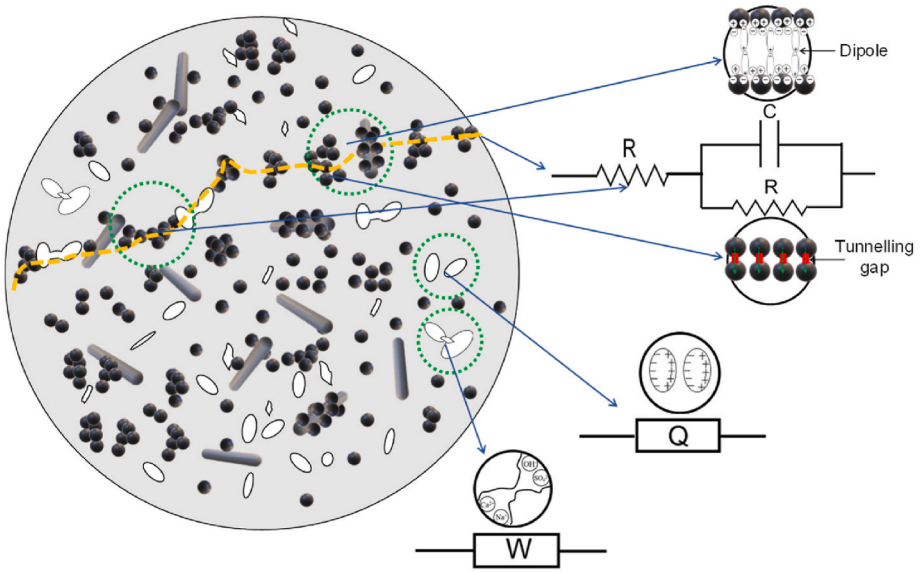

Fig. 11. Schematic diagram of microstructure and equivalent circuit components.

and 20CB as shown in the following Fig. 13. Meanwhile, the diameter of arcs also significantly decreases by an order of magnitude. These variation features of ACIS evidence the significant reduction of material complex impedance, while it is not the case for 05CB02CNF in comparison to 05CB. Thus, the ACIS features shows a good agreement with features of DC resistivity results.

3.4.2. *Equivalent circuit model*

To further examine the conductivity enhancement characteristics and mechanisms of the hybrid inclusion of CNF on CB-based UHPC, the equivalent circuit model comprised by a series of discrete electrical components were analysed based on ACIS. In general, equivalent circuit model is divided into several parts, corresponding to the different conductive behaviours of different phases in composite. Referring to previous relevant studies [66–71], a new equivalent model was proposed based on different conducive phases in the microstructures of materials. The schematic diagram of microstructure and their corresponding equivalent electrical components are illustrated in Fig. 11. For the carbon nanoadditives filled cement composites, tunnelling conduction contributed by very closed adjacent CB/CNF, contact conduction by interconnected CB/CNF and ionic conduction contributed by pore electrolytes mainly govern the conductive behaviour [18,72].

As previously discussed, individual CB/CNF or their agglomerates are tightly embedded in cement matrix, which means there is inevitable coating of matrix phases enclosing the CB/CNF except for those directly connected CB/CNF. The CB/CNF distributed within the matrix is in the form partially conductive path, which contains a certain portion of continuous conductive path and a certain portion of discontinuous conductive path as shown in Fig. 11. To explicate electrical behaviour of partially conductive path, Jiang et al. [70] adopted the $R_0(C_1R_1)$ circuit component to represent partially contacted graphene in cement matrix, where R_0 represented resistance of composite and directly contacted graphene; C_1 and R_1 represented capacitance and resistance of graphene/matrix/graphene structures, respectively. Similarly, Wang et al. [68] adopted a $R_{as}(C_sR_{cs})$ circuit component to explicate the conductive path of partially contacted carbon black aggregates where polymer matrix is as the dielectric, where R_{as} represents the resistance of aggregate, C_s and R_{cs} represents the capacitance and resistance of CB/matrix/CB structures. In this study, the electrical behaviour of directly connected CB/CNF structures and electrolyte resistance by continuously connected micro-pores is represented by a resistor [67,70,73]. The electrical behaviour of unconnected CB/CNF structures and unconnected pores is

explicated by a parallel R–C circuit, showing both the capacitive and resistive behaviours. For the case of plain UHPC, the resistor represents the electrolyte resistance by micro-pore, whereas the capacitor represents the capacitance of insulated matrix.

For the case of single CB and hybrid CB/CNF filled UHPC, the resistor in parallel R–C circuit additionally represents the nonohmic resistance of CB(CNF)/matrix/CB(CNF) structures due to tunnelling effect, in which the adjacent CB/CNF particles are very closely neighbouring for electrons to conquer a potential barrier and allow the tunnelling to take place. Previous studies proposed that the maximum tunnelling distance for electrical current transfer in cement matrix is typically less than several nanometres [74,75]. The capacitor in the parallel R–C circuit represents the sum of the capacitance of insulated matrix and the double layer capacitance generated by CB(CNF)/matrix/CB(CNF) structures. For plain UHPC, the capacitor is only related to the capacitance of insulated matrix. Under the external electric field, the electrical charges will be orientationally deposited along the CB/CNF 'plates' due to the Maxwell-Wagner interfacial polarization, where the matrix between the CB/CNF structures is considered as dielectric, resulting in the formation of a series of tiny electrical double-layer capacitor [76]. Similar capacitive feature has also been discussed in expanded graphite filled cement composite [59]. Nevertheless, the capacitive behaviours only occur in the region where the contact between CB/CNF grains are poor [59,65], with relatively large matrix gap between them that can enable electric charges to be stored. Consequently, the parallel R–C circuit component is essentially controlled by the 'contact state' of CB/CNF structures that are related to the partially conductive paths inside the single CB and hybrid CB/CNF filled UHPC specimens. As the CB content increases, the distance between adjacent CB/CNF structures reduces, accordingly resulting in intensified tunnelling effect and weakened CB(CNF)/matrix/CB(CNF) capacitance.

Based on the discussion, the conductive path contributed by CB/CNF structures and connected pores can be represented by a R(CR) circuit component, that is resistance and capacitive elements conduct electricity in series and parallel. This physical explanation of the parallel R(CR) circuit components is also consistent with the equivalent response models of carbon nanotubes (CNT) cement-based composites [73,77]. In addition, the ions chemically or physically absorbed in the interfacial area between pores and matrix, the opposite charges at the solid layer and the by solid-liquid bilayer also act as double-layer capacitance unit, as so called 'solid-liquid interface capacitance' under AC [78–80]. However, owing to the complex nature of unconnected pores such as different shape, size, pore structure and their moisture content, their time constant response to different frequency ranges are different, leading to 'dispersion effect' in ACIS [28,81]. Consequently, the complex unconnected pores cannot be considered as a perfect capacitor but instead are represented by a constant phase element (CPE, expressed by Q) [69], and its formula is illustrated in Eq. (8).

$$Z_Q = \frac{1}{Y_0 \omega^n}\left(cos\frac{n\pi}{2} - jsin\frac{n\pi}{2}\right) \tag{8}$$

where Z_Q denotes the impedance (Ω), $\omega = 2\pi f$ denotes angular frequency, Y_0 represents capacitance or resistance, when $n = 1$, CPE behaves as ideal capacitor with the capacitance of $C = Y_0$, when $n = 0$, CPE behaves as ideal resistor with the resistance of $R = 1/Y_0$, when $0 < n < 1$, CPE has the both capacitive and resistive behaviors.

It is worthy to note although the UHPC specimens was dried at 60 °C oven for 24 h to eliminate the ionic conductivity, there is still certain moisture inside UHPC specimen, and the ionic conductivity still plays an important role in the UHPC as evident by later piezoresistivity test result of plain UHPC. This is probably related to the complex types of water in pores and the drying treatment only evaporate part the of bulk capillary water [82]. The water evaporation alters the ionic centration and internal diffusion inside the cement composites [83]. For the partially saturated specimens, the charge transfer and ion diffusion not only go through the interconnected solids or continuous fluids but also through the interface region of solid-liquid phases [84]. Thus, the diffusion impedance of ion diffusion in the solution stemming from gradient of ion concentration should also take into consideration. The diffusion effect is often represented by Warburg impedance [69,85], and is formula is shown in Eq. (9).

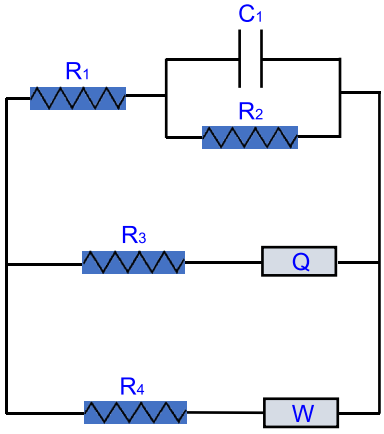

Fig. 12. Equivalent circuit model.

$$Z_w = \frac{\sigma}{\sqrt{\omega}} - j\frac{\sigma}{\sqrt{\omega}} \tag{9}$$

where Z_w denotes Warburg impedance and σ denotes Warburg coefficient.

Based on the analysis of the microstructure and the involved conductive behaviors, the overall equivalent circuit model is illustrated in Fig. 12, which is expressed as $((R_1(C_1R_2))(R_3Q)(R_4W))$ and its impedance formula is shown in Eq. (10)

$$\frac{1}{Z} = \frac{1}{R_1 + \frac{R_2}{1+\omega^2 R_2^2 C_1^2} - j \bullet \frac{\omega R_2^2 C_1}{1+\omega^2 R_2^2 C_1^2}} + \frac{1}{R_3 + Z_Q} + \frac{1}{R_4 + Z_w} \tag{10}$$

where Z denotes bulk UHPC impedance; C_1 represents the capacitive behaviour of the insulated matrix and CB(CNF)/matrix/CB(CNF) structures; R_1 represents the electrical behaviour of directly connected CB/CNF structures and connected pore solution; R_2 represents the electrical behaviour of directly connected CB/CNF structures and connected pore solution. Z_Q represents the electrical behaviour of complex unconnected pore structure; R_3 represents the bulk resistance in series with the unconnected pore in the direction of electrical current and 'R_3+Z_Q' is presented as 'oblique line' in the Nyquist plot; Z_w represents the electrical behaviour of ions diffusion; R_4 represents the bulk resistance in series with charge-diffusion layers in the direction of electrical current, 'R_4+Z_w' is presented as a 'depressed semi-circle' in Nyquist plot.

It is shall be noted that different from many previous studies [86], polarization behaviours at the sample-electrode interface which are irrelevant to the electrical conductivity analysis are discarded in this model to minimize the circuit elements. Essentially, they will not provide any significant information concerning the conductive behaviour in CB/CNF filled cement system [87]. Therefore, only the impedance spectra with the frequency from 10 Hz to 1.0 MHz are fitted by the proposed model. Fig. 13 shows the model $((R_1(C_1R_2))(R_3Q)(R_4W))$ fitting curves for single CB and hybrid CB/CNF filled UHPC samples. The model fitting curves show the good coincidence degree with the experimental impedance data, which is supported by the highest chi-squared (Chsq) value of 1.02E-4 [19,69]. The smaller the Chsq value, the better the fitting degree. It is worth noting that the fitting degree of the low-frequency semicircle is relatively poor compared to that of the high-frequency semicircle (see the zoomed sub-graphs in

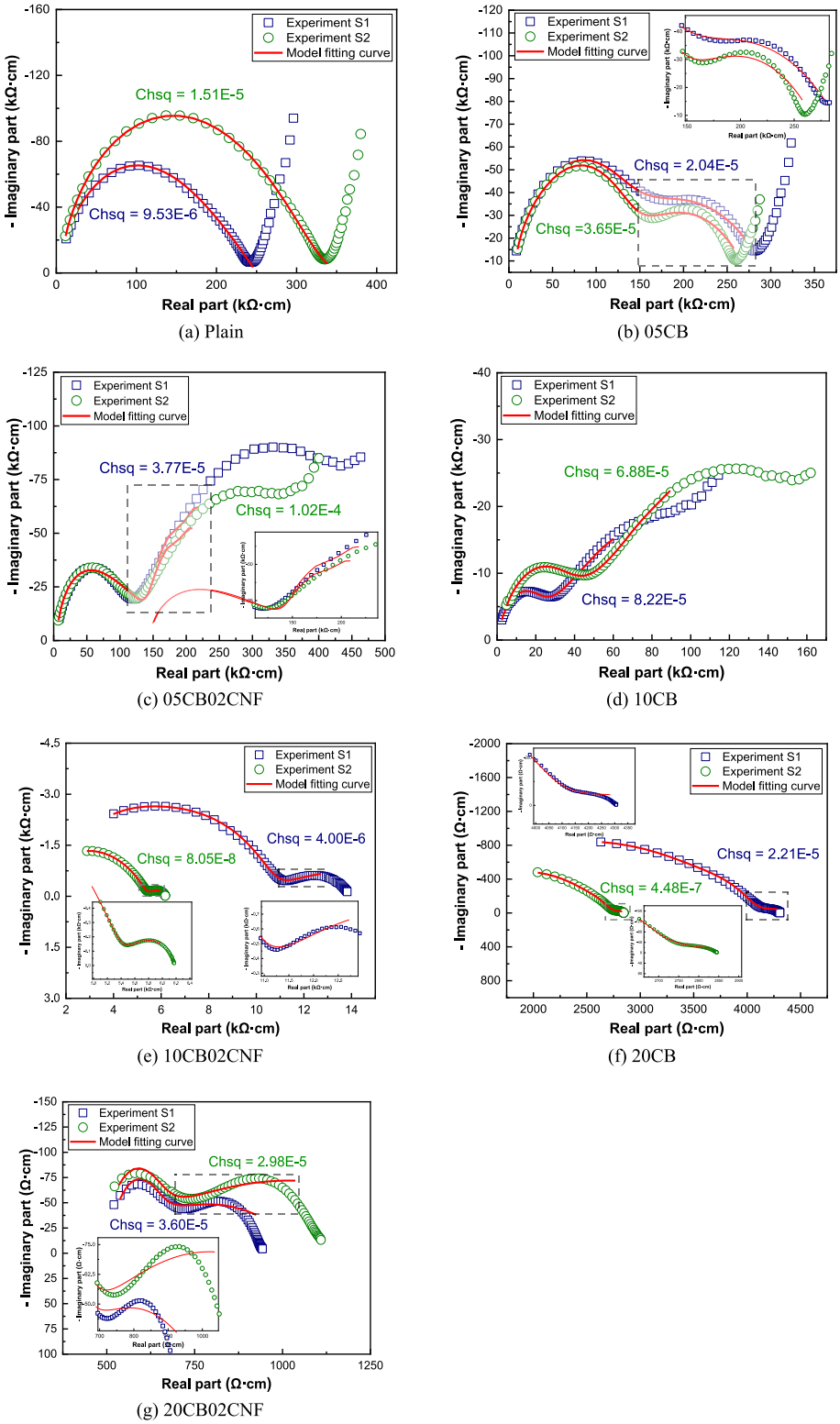

Fig. 13. Nyquist plots and equivalent circuit model fitting curves.

Fig. 13). This observation aligns well with the fact that the low-frequency semicircle is associated with the electrochemical reactions of the cementitious matrix, such as the charge diffusion process in the pore electrolyte and the charge interaction of the solid/liquid double phase, which possess an unstable and complex nature. Therefore, the proposed model ($(R_1(C_1R_2))(R_3Q)(R_4W)$) possesses a superior feasibility for modelling the electrochemical behaviours involved in single CB and hybrid CB/CNF filled UHPC samples.

3.4.3. *Analysis of equivalent circuit parameters*

Table 4 shows the fitting parameters of the proposed model ($(R_1(C_1R_2))(R_3Q)(R_4W)$). As shown in Fig. 14, the resistance value R_1 of plain samples to 05CB is nearly unchanged, the resistance value R_2 drops by about two-thirds, and the dielectric capacitance value C_1 slightly

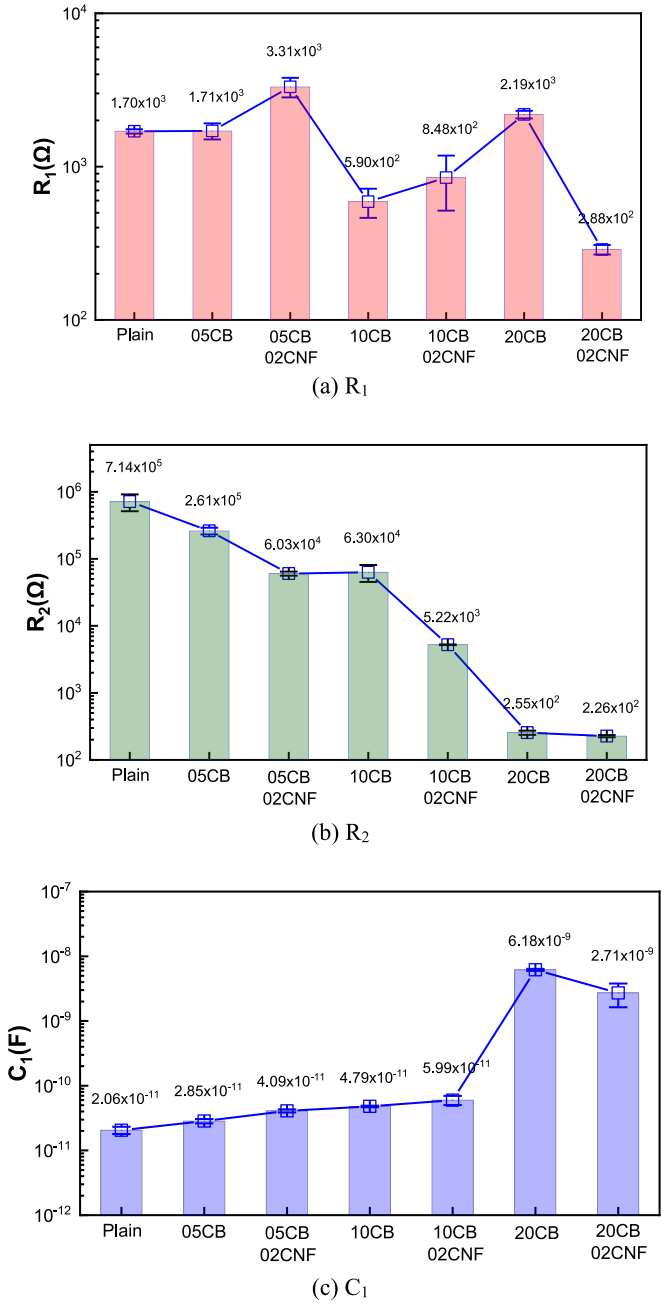

Fig. 14. Variations of equivalent circuit model fitting parameters for single CB and hybrid CB/CNF filled UHPC.

increases. These variations are well consistent with the fact that the dosage of 0.5 % CB is at the starting percolation threshold. There is no continuous conductive path formed by CB particles/agglomerates as a consequence of inadequate concentration of conductive fillers [88]. The addition of 0.5 % CB does not contribute to additional continuous conductive path compared to connected pores filled with electrolyte in plain samples. In such a case, the resistance value R_1 is merely varied and only resistance value R_2 drops since 0.5 % CB particles/agglomerates dispersed in cement matrix in discontinuous form and only contribute the tunnelling conduction. From 05CB to 05CB02CNF, the resistance value R_1 almost doubles, the resistance value R_2 drops by about three-fourths. The increase in R_1 should attribute to refined pore structure, which blokes the continuous conductive paths in certain range [87,89]. The increase in R_1 is also observed in the case form 10CB to 10CB02CNF, which probably reveals the beneficial role of CNF in modifying the microstructures. The unexpected larger R_1 value for 20CB compared to 10CB is probably owing to higher occurrence of localized defects due to increasing CB agglomerates in 20CB, which blocks the formation of continuous pathways to certain extent [26,53]. As R_1 increases, there is obvious decrease in R_2 for both cases from 05CB to 05CB02CNF and from 10CB to 10CB02CNF. Especially for the case from 10CB to 10CB02CNF, there is a significance decrease in R_2 by nearly one order of magnitude.

These variations indicate that the incorporation of 0.2 % CNF mainly contributes to the conductive network in the form of increasing tunnelling conduction (discontinuous conductive paths) for the cases of 05CB02CNF and 10CB02CNF. However, different trends are observed from 20CB to 20CB02CNF, in which case R_2 is nearly unaltered while R_1 critically drops to near one order of magnitude. This implies that the incorporation of 0.2 % CNF mainly contributes to the conductive network in the form of increasing contact conduction (continuous conductive paths) for the case of 20CB02CNF. These variation trends agree well with conductive characteristics shown in microstructures. For the cases of 05CB02CNF and 10CB02CNF, CB particles/agglomerates are sparsely distributed in the matrix without forming a continuous percolating network. Although the fibrous CNF with high aspect ratio can play a crucial role as long-range conductor and fill the dielectric gap between CB, they mainly achieve the cooperative improvement effect in electrical conductivity by narrowing the dielectric gap between adjacent CB particles/agglomerates and enhancing the tunnelling conduction.

When compared with the case from 05CB to 05CB02CNF, the significant drop in R_2 for the case from 10CB to 10CB02CNF evidences more efficient improvement in tunnelling conduction, which is consistent with the fact that more conductive contact points provided by higher dosage of 1.0 % CB [36]. The distinctive synergetic improvement efficiency in electrical properties brought by CNF on CB/UHPC samples filled with different dosage of CB can be related to the percolation characteristics. When CB content approaches to the start of percolation threshold (i.e., 0.5 % CB), the CB marginally distributed in matrix can provide limited conductive contact points. When CB content within percolation zone (i.e., 1.0 % CB) where the tunnelling distance becomes the dominant factor [90], the assistance of CNF shows the most efficient synergetic improvement in electrical properties. The contribution of tunnelling conduction provided by CNF in 05CB02CNF even cannot overcome the reduced conduction by refined porosity structure, which leads to increase in bulk resistivity from 05CB to 05CB02CNF. When CB content approaches to the end of percolation zone (i.e., 2.0 % CB), the CB particles/agglomerates already broadly distribute and form percolating conductive network in the matrix, in this case CNF mainly helps form the continuous conductive path and contribute to contact conduction rather than tunnelling conduction.

The above hypothetical analysis is further supported by the variation trend of capacitance value C_1. From plain samples to 10CB02CNF, there is a continuous increase in C_1, but the increasing range is limited within the same order of magnitude. As previously discussed, C_1 is assigned to the capacitance of insulated matrix and the double layer capacitance of CB(CNF)/matrix/CB(CNF) structures due to polarization at CB(CNF)/matrix interfaces. That is the incorporation of conductive fillers into humidified matrix generates a numerous 'tiny double layers' with high specific capacitance that are added into cement matrix [89,91]. It is worthy mentioned although the characteristic time constant corresponding to such two electrochemical responses are different, which is evidenced by the non-symmetrical variations in electrical parameters and can lead to changes in the time constant [89], the variation trend of C_1 is directly linked to the effects of the incorporating CNF/CB. An example is the variation of C_1 is far remarkably less than the variation of R_1 from plain sample to 10CB02CNF. When the dosage of CB/CNF is low, before reaching the percolation threshold, the numerous 'tiny double layer capacitor' by individual CB(CNF)/matrix/CB(CNF) structure can be anticipated to be connected in parallel, which is stemmed from the fact that the current from one local CB(CNF)/matrix/CB(CNF)

Table 4
Fitting parameters of equivalent circuit model.

Group	Parameters	R_1 (Ω)	R_2 (Ω)	C_1 (F)	R_3 (Ω)	Z_W (Ω)	R_4 (Ω)	Z_Q		Regression SS
	Samples							Y_0	n	
Plain	S_1	1660	8.56E+5	2.24E-11	11465	48797	22542	7.03E-8	0.416	0.00140
	S_2	1737	5.72E+5	1.87E-11	8754	1.02E+5	1.24E+5	2.38E-7	0.192	8.76E-4
05CB	S_1	1563	2.82E+5	3.00E-11	**0.0493**	90647	47179	2.33E-7	0.448	1.87E-3
	S_2	1853	2.40E+5	2.69E-11	**2.06E-4**	86283	58795	2.27E-7	0.484	8.64E-4
05CB02CNF	S_1	3654	63241	3.93E-11	95941	7.56E+6	8374	7.52E-7	0.292	0.0292
	S_2	2970	57294	4.24E-11	1.04E+5	3.71E+6	5896	5.13E-7	0.332	0.0209
10CB	S_1	500.6	50422	4.88E-11	**2.26E-5**	3.43E+5	8431	1.74E-5	0.354	7.59E-3
	S_2	680.2	75568	4.70E-11	1411	1.64E+6	10607	1.34E-5	0.324	6.33E-3
10CB02CNF	S_1	1082	5180	5.30E-11	**2.85E-4**	107674	5795	6.38E-5	0.258	3.69 E−4
	S_2	613.1	5267	6.67E-11	419.5	1468	9185	6.85E-6	0.483	7.41E-6
20CB	S_1	2099	267.9	6.34E-09	2482	**3.80E-6**	754.1	1.95E-4	0.0405	2.03E-4
	S_2	2276	241.9	6.02E-09	239.8	693	603.3	5.29E-5	0.0804	4.40E-5
20CB02CNF	S_1	273.1	232.2	3.47E-09	402.3	288	230.9	3.19E-4	0.219	3.32E-3
	S_2	302.3	220.3	1.95E-09	533.4	797.7	154.5	9.24E-4	0.166	2.75E-3

Note: Regression SS means the regression sum of squares, which reflects how well a fitting curve represents the fitting data. A higher regression SS indicates the fitting curve does not fit the data well. The bolds values denote the abnormal values.

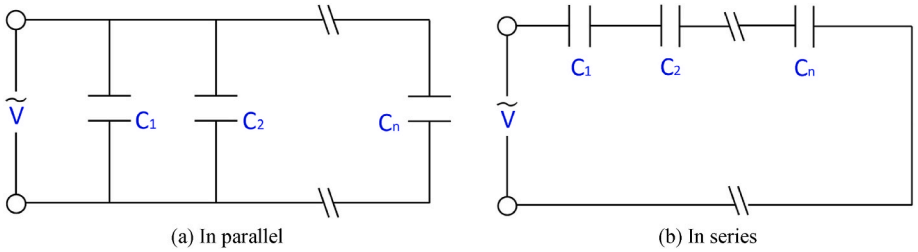

Fig. 15. Circuit of CB(CNF)/matrix/CB(CNF) capacitors.

capacitor to the adjacent populated one does not follow a single channel, but follows multiple channels as shown in Fig. 15 (a) [27,91,92]. In this case, the capacitance contributed by CB(CNF)/matrix/CB(CNF) structures can be evaluated by Eq. (11).

$$C_p = \sum_{i=1}^{n} C_i \tag{11}$$

where C_i is the capacitance of localized capacitor and can be evaluated based on Eq. (12).

$$C_i = A \bullet k \frac{\varepsilon}{d} \tag{12}$$

where A is the area of individual CB/CNF structure; k is the relative permittivity of dielectric mortar; ε is the permittivity of space; d is the distance between two CB/CNF structures. According to Eqs. (11) and (12), C_i increases with the increase of CB/CNF dosage since A increases and d decreases. In addition, since the number of CB(CNF)/matrix/CB(CNF) capacitors increases with the increase of CB(CNF) dosage, C_p increases. Therefore, there is a gradual and steady increase in C_1 from plain samples to 10CB02CNF. Interestingly, there is dramatic increase in C_1 by approximately two orders of magnitude from 10CB02CNF to 20CB. This is probably related to the presence of increasing number of CB agglomerates. Compared with dispersed CB/CNF, the presence of CB/CNF agglomerates form the bigger CB(CNF) agglomerate/matrix/CB(CNF) agglomerate capacitors that are associated with higher storage capacity and larger capacitance values [91]. The increase in capacitance with the increasing concentration of conductive fillers before reaching percolation threshold is also detected in previous studies [27,59]. In addition, there is a sudden decrease in C_1 from 20CB to 20CB02CNF, which should be related to the fact the number of CB(CNF)/matrix/CB(CNF) capacitors is assumed to connect in series when dosage of CB/CNF approach percolation threshold as illustrated in Fig. 15 (b). In this case, the charge can only be stored in the local regions where the contact of CB/CNF structures is poor and the capacitance C_s can be evaluated by Eq. (13):

$$C_s = \frac{1}{\sum_{i=1}^{n} \frac{1}{C_i}} \tag{13}$$

According to Eq. (13), increase of individual local C_i is equivalent to decrease of C_s. Consequently, the capacitive character weakened from 20CB to 20CB02CNF reveals the fact that the incorporation of CNF reduces the regimens where contact of CB/CNF is poor. This agrees well with the previous hypothesis that synergetic improvement of CNF on the electrical conductivity of 20CB is mainly helped make up the continuous conductive paths and contributing to the contact conduction. The consistent findings by analysing the variations of different electrical parameters should validate the proposed equivalent circuit model.

Overall, the proposed model based on conductive phases involved in microstructures can provide reliable information to characterize the conductive behaviours, showing a close agreement with the results of microstructural characterization. The inherent behaviours of CNF, as long-range conductor to play the role to achieve the synergetic improvement effect in electrical properties for single CB filled UHPC with different CB dosage, can be successfully analysed based on variations of equivalent circuit parameters. When the dosage of CB approaches to the start of percolation zone (e.g., for the cases of 0.5 % and 1.0 % CB), CNF mainly assist in forming discontinuous conductive paths, narrow the gap between neighbouring CB structures, and contribute to the tunnelling conduction. These characters can be reflected by the increase in nearly unchanged/increase in R_1, decrease in R_2 and increase in C_1. Particularly, a comparably significant drop in R_2 and increase in C_1 for the case from 10CB to 10CB02CNF in comparison to the case from 05CB to 05CB02CNF, indicating much higher efficiency of synergetic improvement effect brought by the inclusion of CNF on 10CB than on 05CB, which can be closely correlated to percolation characteristics and the microstructures.

When the CB dosage approaches the percolation threshold (i.e., 2.0

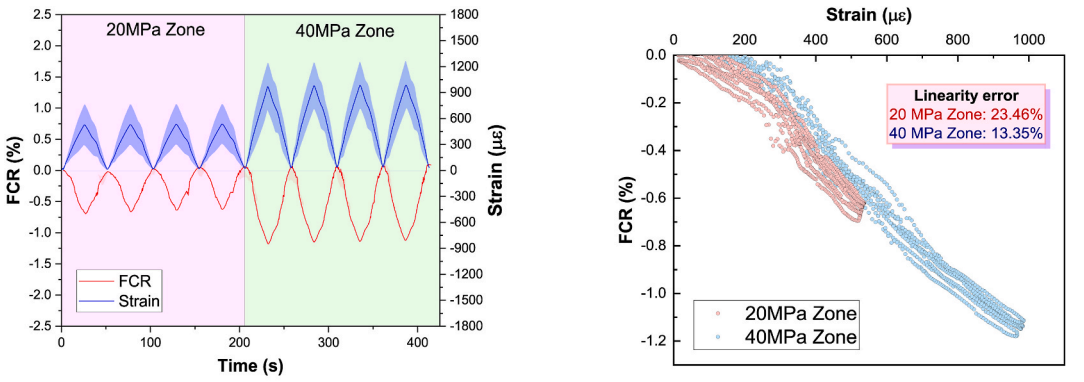

(a) Plain

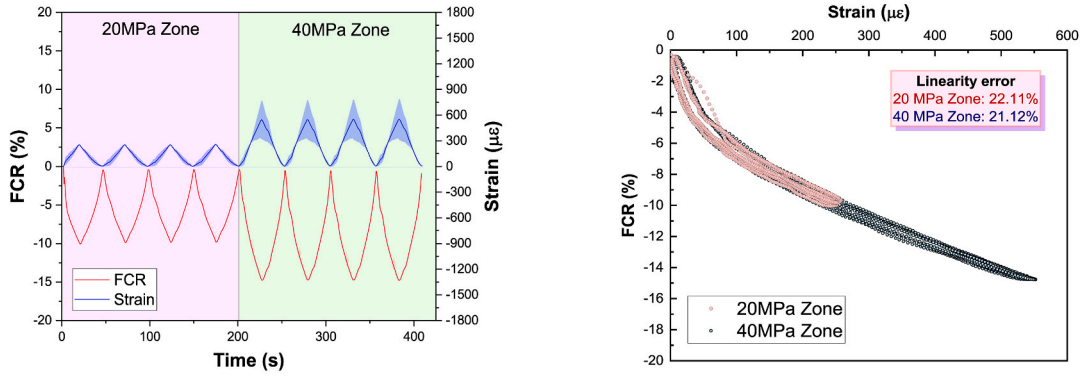

(b) 05CB

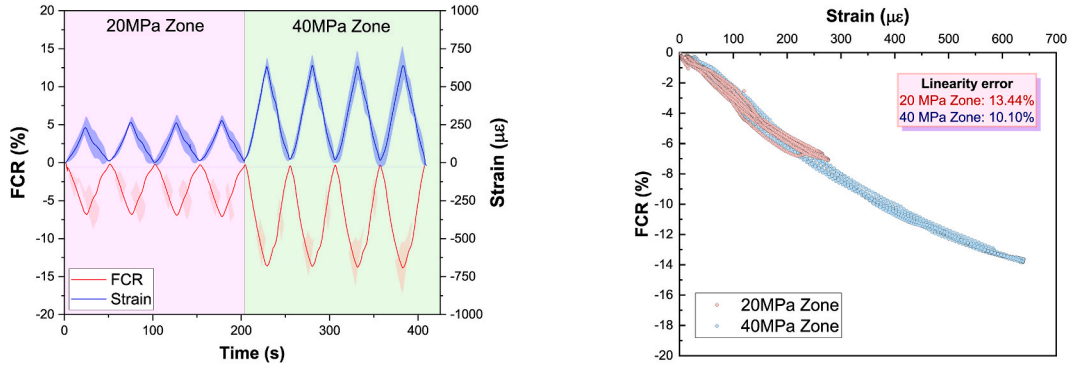

(c) 05CB02CNF

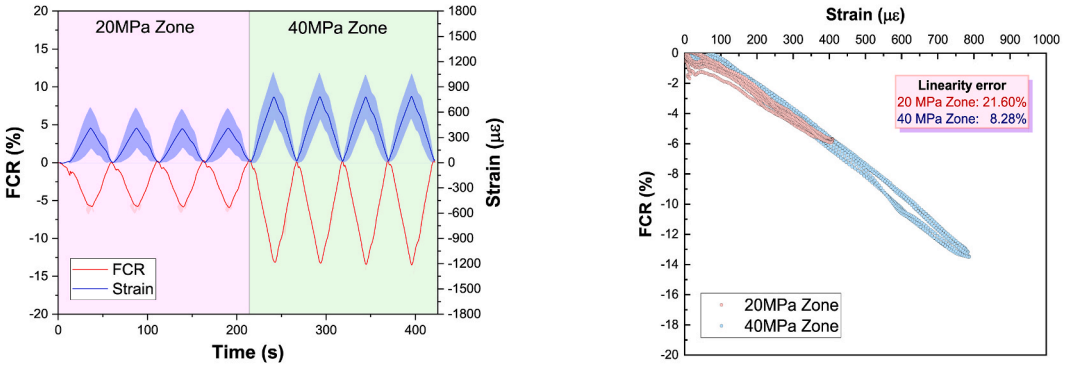

(d) 10CB

Fig. 16. Piezoresistive sensing performance for all groups under quasi-static cyclic loading.

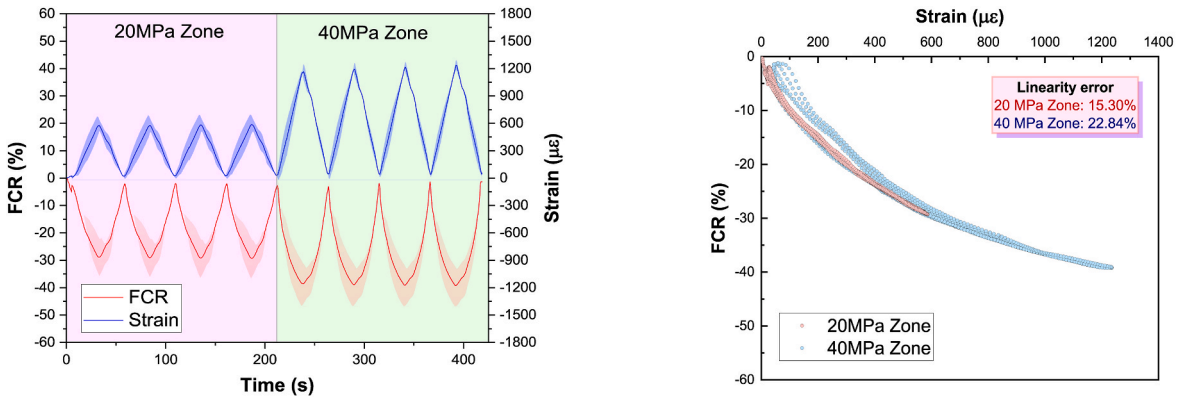

(e) 10CB02CNF

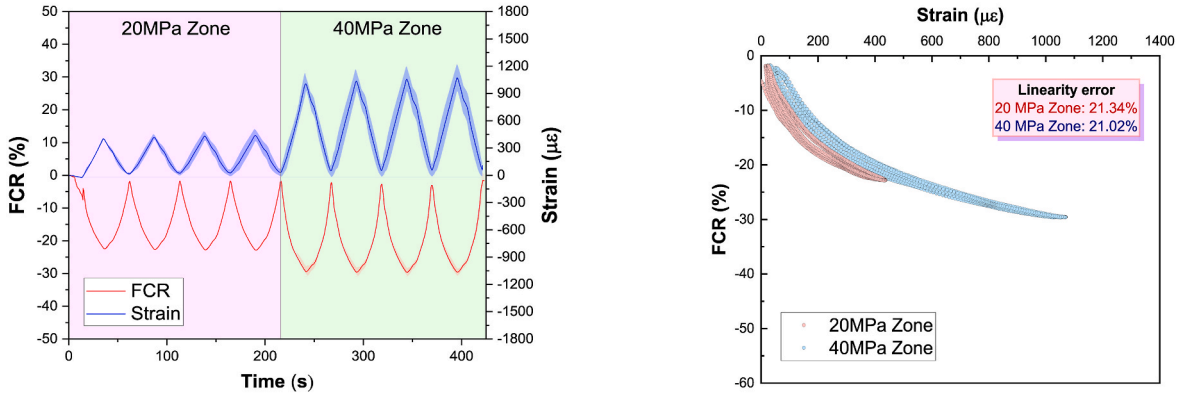

(f) 20CB

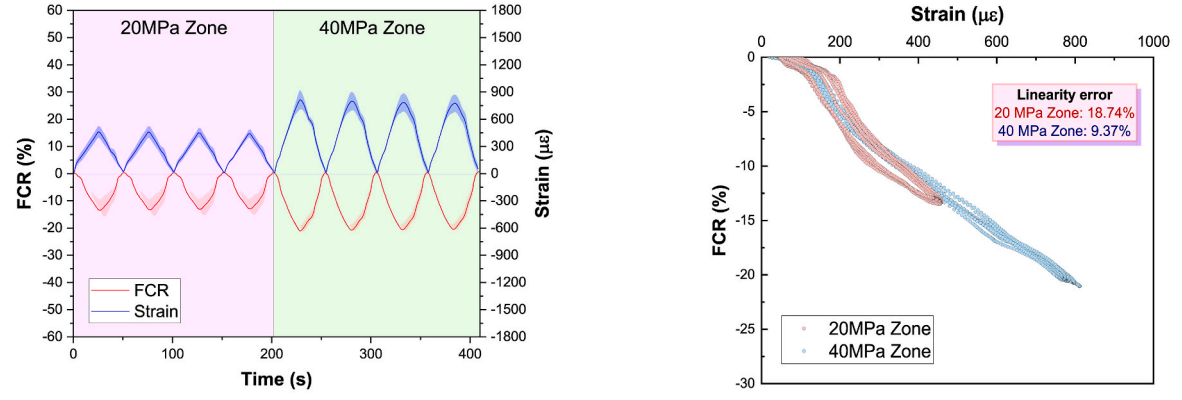

(g) 20CB02CNF

Fig. 16. (*continued*).

% CB), CNF mainly assist in forming continuous path, directly connect the neighbouring CB structures, and contribute to contact conduction. These characters can be reflected by decrease in R_1, nearly unchanged in R_2, and decrease in C_1. Thus, the essential information concerning conductive behaviours of single CB and hybrid CB/CNF filled UHPC can be properly extracted from a semi-qualitative point of view, based the variations of equivalent circuit parameters that are assigned to different electrical phases involved in the microstructures. The obtained essential information such as the percolating state of CB and the different forms of how CNF contribute to conductive network in hybrid CB/CNF filled smart UHPC can help understand the conductive behaviours and working mechanisms at microstructural level, which can provide new insight into the material design strategy for enhancing the electrical and sensing performances of UHPC-based cementitious sensors.

3.4.4. *Strength and limitations of proposed model*

The microstructure models established for the ACIS data interpretation of cement-based material can be classified into layer model, brick model, T and I model, barrier/pin-hole model, and conductive path model [28]. The proposed circuit model in the present study is classified as the conductive path model, which possesses the advantage of simulating the real distribution of various electrical phases and having the clear physical meaning pertaining to individual components [28,30]. The theory regarding the elements assignment (assigning the physical meaning to each parameter of the equivalent circuit) and model establishment (continuous conductive path, discontinuous conductive path

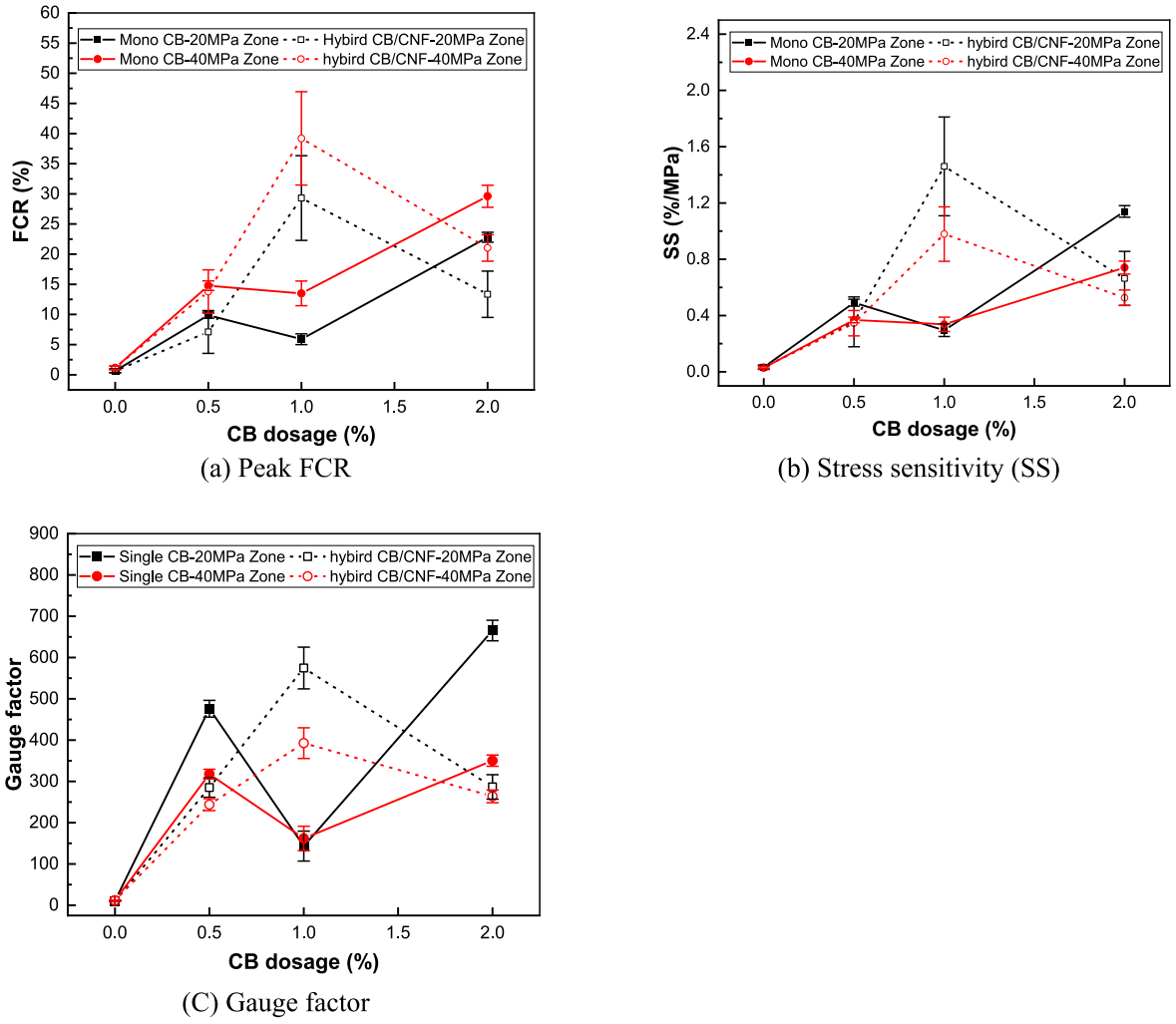

Fig. 17. Variations of self-sensing sensitivities of single CB filled and hybrid CB/CNF filled UHPC under quasi-static cyclic loading.

and insulation path) is referred to and further modified based on serval conductive path models previously developed [67,69,93]. However, it is worthy pointing out that although the proposed equivalent modelling circuit is assigned according to microstructural phases of cementitious materials, the resultant parameters often do not consider the geometrical features of the conductive inclusions and their volume fraction [60]. In addition, the appearance of the ACIS dispersion phenomenon in cement-based materials still perplexes their effect on data interpretation [28]. Multiple equivalent circuit models may be capable of fitting and regenerating the experimental data [60]. A single equivalent model can hardly to completely represent the electrical behaviours in the complex microstructure of cement-based materials [79,94]. These influential factors may potentially comprise the reliability of the proposed model [94].

The development of equivalent circuit models, especially for cement-based sensors, is still at the budding stage; each model is established and interpreted in various ways, which has certain limited applicability [58,79]. Due to the different conductive systems comprised by multi-phase, multi-scale, and multi-dimension functional fillers, there is an absence of a universal conductive theory and a generalized model. In the present study, the proposed model is reasonably established by individually assigning the circuit elements to the conductive microstructures and validated by the fitting degree and analysis of variations in model parameters. The extracted information is mutually well aligned with the conductivity, percolating state, microstructural characterization and piezoresistive sensitives. Further efforts could be put on the aspects of establishing a more generalized model with extended applicability and reliability, separating the averaging and mixing effects of the ACIS for the interpretation of individual and conductive characteristics, the application potential of differential impedance analysis (DIA) [95,96], etc, to further advance the ACIS as a promising non-destructive technique in accurately characterize the electrical microstructures in cement-based sensors.

3.5. *Piezoresistive performance*

3.5.1. *Quasi-static cyclic loading*

The piezoresistive sensing responses and the associated linear errors of single CB filled and hybrid CB/CNF filled samples are shown in Fig. 16. The selective maximum stress amplitude of 40 MPa is inconsistent with previous studies examining the smart UHPC samples [97], which is significantly higher than typically used in studies concerning normal concrete/mortar/paste samples, thus indicating the favourable high load sensing capability of smart UHPC. Generally, both single CB filled, and hybrid CB/CNF filled samples present a satisfactorily repeatable and reversible piezoresistive responses with good synchronicity, although the responses of some samples show a certain degree of nonlinearity. In comparison to the single CB filled samples, the piezoresistive responses of hybrid CB/CNF filled samples shows more excellent reparability and hysteresis than single CB filled samples. The piezoresistive response of plain sample with very limited FCR values indicate the role of ionic conduction [53], which is consistent to the result of

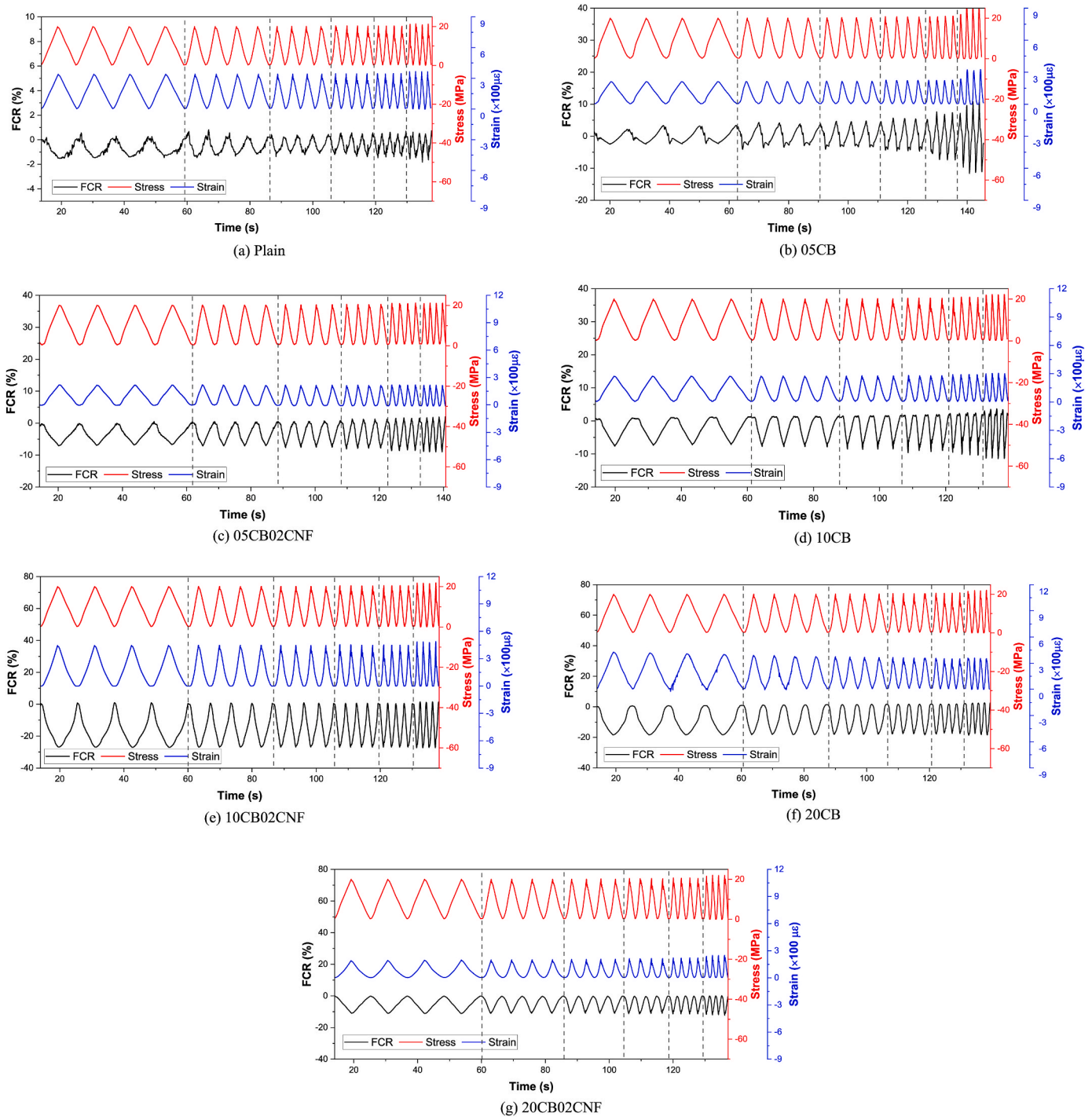

Fig. 18. Piezoresistive sensing performance for all groups under dynamic cyclic loading.

equivalent circuit analysis. The variations of sensitivity indicators including peak FCR, stress sensitivity (SS) and gauge factor (GF) and FCR-strain responses are illustrated in Fig. 17, which were calculated based on the mean FCR-stress and FCR-strain responses under both 20 MPa and 40 MPa stress amplitude regions. It is seen that the sensitivities of 05CB02NCF are roughly kept at a similar level compared to 05CB, which can be reflected by the absolute peak FCR value under 40 MPa regime is roughly 14 % for both 05CB and 05CB02CNF in Fig. 16 (b) and (c). There is one exception for the case of 05CB under the 20 MPa regime as shown in Fig. 17 (c), which is induced by the fact that GF is calculated based on the slope of linear fitting equations of data scatters in FCR-strain curves while 05CB presents a severe nonlinear piezoresistive response. Differently, 10CB02CNF shows distinctive higher sensitivities than 10CB, as substantiated in Fig. 17. The absolute value of peak FCR under 40 MPa regime is approximately 39 % for 10CB02CNF, which is almost trebled compared to the counterpart of 10CB in Fig. 16 (d) and (e). With further increase of CB dosage to 2.0 %, the 20CB02CNF shows the reduced sensitivities compared to 20CB in Fig. 17 and Fig. 16 (e) and (f). It is revealed that when CB dosages below the percolation threshold (i.e., 0.5 % and 1.0 % CB), the CNF mainly contributes to the conductive network in the form of enhancing the tunnelling conduction. For the CB dosage of 0.5 % which approaches to the start of percolation, the individual CB/CB agglomerates are sparsely distributed in the matrix and the gaps between adjacent CB structures are relatively large.

Therefore, incorporation of CNF cannot efficiently fill gaps between adjacent CB and contribute to tunnelling conduction. However, when the CB dosage increases to 1.0 % which is within the percolation, the gaps between adjacent CB structures reduce and tunnelling conduction start to dominate the conductive behaviours [98]. When CB content further increases to 2.0 % which approaches to the end of percolation, there is already percolating CB conductive network inside the matrix, the incorporation of CNF can directly link or bridge the adjacent CB structure over a long range and mainly contribute to the enhanced contact conduction. In this case, although the resistivity of 20CB02CNF still drops when compared to 20CB, its piezoresistive response presents the reduced sensitivities. The reduced sensitivities should be attributed to the fact that there is pre-established percolating network in 20CB whereas 20CB02CNF is associated with a denser conductive network. When dense conductive network is already formed in specimens before loading, the electrical pathways will be less altered towards applied loading, leading to reduced sensitivities [11]. Therefore, it seems that the most effective synergetic effect of CNF for hybrid CB/CNF filled UHPC compared to single CB filled UHPC is achieved when CB content is within the percolation zone. In this case, the fibrous CNF as long-range conductor interspersed among the adjacent CB structures, forming the CB(CNF)/matrix/CB(CNF) structures with dielectric gap that are sufficiently small to enable the tunnelling conduction.

Consequently, the significant change of tunnelling resistance contributed by enhanced tunnelling conduction for 10CB02CNF compared to 10CB should be mainly responsible for its greatly improved sensitivities in piezoresistive response, which is consistent with the fact that change of tunnelling distance between conductive fillers is a dominant factor responsible for the piezoresistive response of the cement-based sensors within the percolation zone [98]. According to tunnelling theory [18,99], the tunnelling resistance has an exponential correlation with the distance between adjacent conductive fillers (barrier width). The local tunnelling resistance (R) as a function of the distance between adjacent conductive fillers (d) can be expressed by Refs. [98,100] as Eq. (14):

$$R = \frac{d\hbar^2}{Ae^2\left(2m\sqrt{\lambda}\right)} \bullet \exp\left(\frac{4\pi d}{\hbar} \bullet 2m\sqrt{\lambda}\right) \tag{14}$$

where e and m are electric charge and mass of an electron, respectively; h is Plank's constant; λ is the potential barrier height, A is the function area of two adjacent conductive fillers. In the loading stage, the distance between adjacent CB(CNF) structures decreases and tunnelling resistance decreases; In the unloading stage, the distance between adjacent CB(CNF) structures increases and tunnelling resistance increases. Overall, the variations trend of sensitivities for the piezoresistive responses of hybrid CB/CNF filled UHPC compared to single CB filled UHPC shows a good coincidence with conductive behaviours extracted from the analysis of percolation threshold, electrical microstructure, and equivalent electrical circuit. In addition, numerous previous studies have observed that the sensing effectiveness of self-sensing UHPC filled with steel fibers and carbon nanotubes is more efficient under tensile stress states than compressive stress states due to the relatively dense microstructures [101–103]. The relatively sensitive piezoresistivity in response to compression of CB/CNF UHPC in this study is likely related to the synergistic effect of several factors, such as a relatively low dosage of quartz sand and the absence of fibre additives like steel fibres/wires. The increased sand ratio and the presence of steel fibres improve the elastic modulus of UHPC, resulting in reduced deformation under identical compression loading levels. The relatively effective sensing characteristics of CB/CNF-filled UHPC under compression align well with findings from a previous study on CB-filled UHPC [52]. Future studies should preferably aim to verify the evolution of the elastic modulus both experimentally and numerically in the presence of fibre additives.

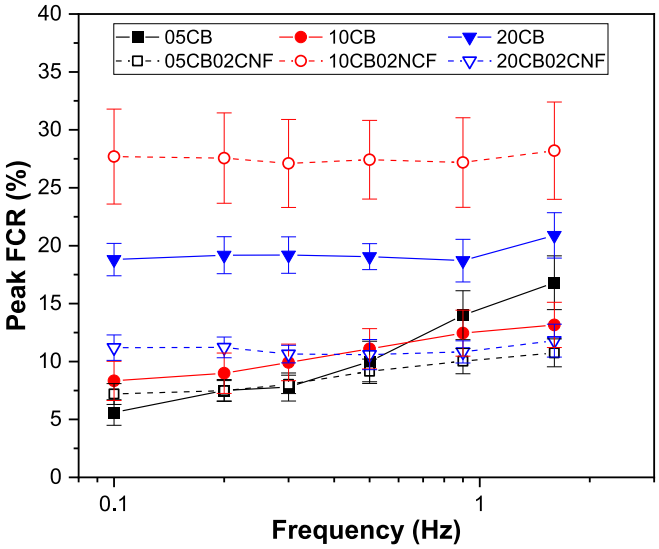

Fig. 19. Variations of peak FCR values for single CB and hybrid CB/CNF filled UHPC under dynamic cyclic loading with different loading frequencies.

3.5.2. *Dynamic cyclic loading*

Apart from quasi-static loading condition, the competent piezoresistive responses of cement-based sensors under dynamic loading condition are of vital importance for dynamic structural monitoring and traffic monitoring applications [30,31,104]. The piezoresistive responses for all groups are illustrated in Fig. 18. Although parallel specimens were tested, the variation of sensitivities for different groups are generally consistent with piezoresistive responses under quasi-static load. The plain sample and 05CB show the unsatisfactory piezoresistive response with zigizg characteristic, demonstrating poor stability and repeatability, which is attributed to the fact ionic conduction dominates the conductive phase. The pore solution-based conductive network is easily disturbed under dynamical compressive loading, which is consistent to the result previously reported that the stability of electrical resistivity of CNT filled UHPC under dynamic loading improved as the increase of CNT content [11]. To evaluate the stability of piezoresistive response under dynamic cyclic loading with different frequency, Fig. 19 summarized the variations of mean peak FCR for single CB filled and hybrid CB/CNF filled UHPC with increasing frequency. The peak FCR values for the groups 10CB02CNF, 20CB, and 20CB02CNF is merely altered with the increasing frequency compared to the counterparts for groups 05CB, 05CB02CNF and 10CB. The slightly higher peak FCR value under the highest frequency of 1.6 Hz is due to the limitation of compression machine, which induces the slightly higher loading amplitude than 20 MPa. The peak FCR values for the groups 05CB, 05CB02CNF and 10CB exhibits an obvious increasing trend with the increasing frequency, especially for 05CB. The increasing trend for the groups with less CB/CNF content show a good agreement with the relevant literature that studied the self-sensing performance of graphene oxide reinforced cement composites under dynamic cyclic loading with the identical loading frequency range, which is attributed to the fact that polarization effect takes place at lower frequency [31]. Overall, it is indicated that the self-sensing performance for cement-based sensors with lower conductive filler is more vulnerable to the dynamic cyclic loading with various loading frequencies because of the sparely conductive networks, which is more easily disturbed and may not precisely response to applied loading with increasing frequency. The stability of piezoresistive sensing performance in response to dynamic cyclic load improves with increasing content of conductive fillers.

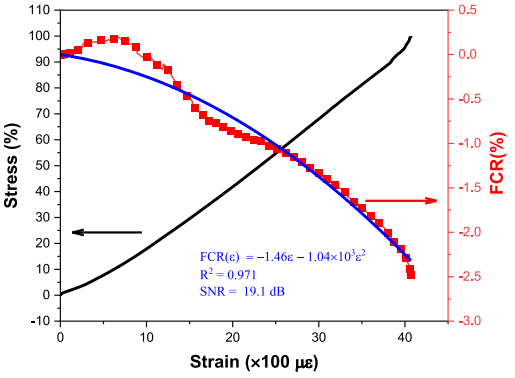

(a) Plain

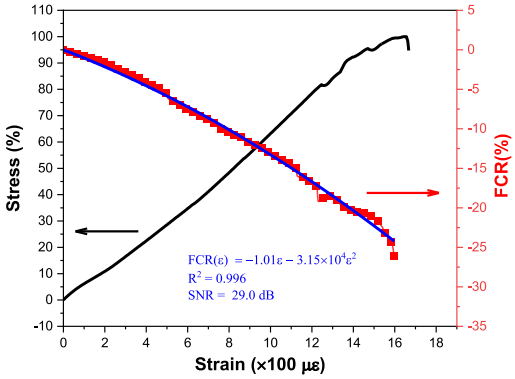

(b) 05CB

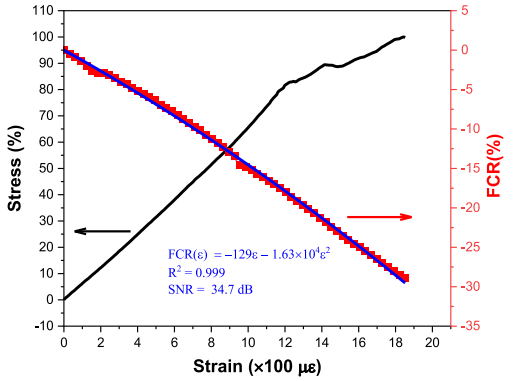

(c) 05CB02CNF

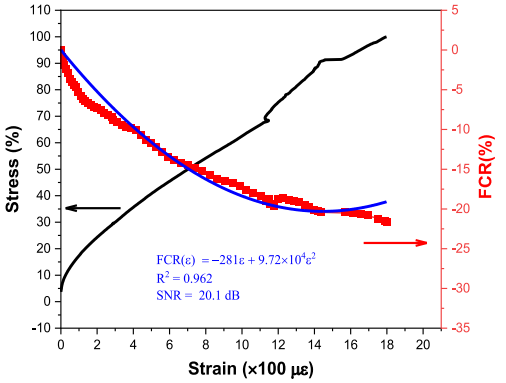

(d) 10CB

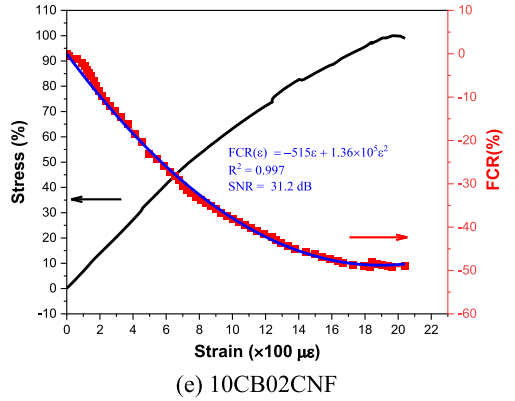

(e) 10CB02CNF

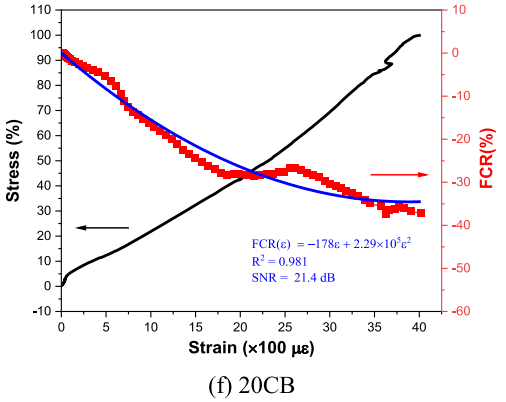

(f) 20CB

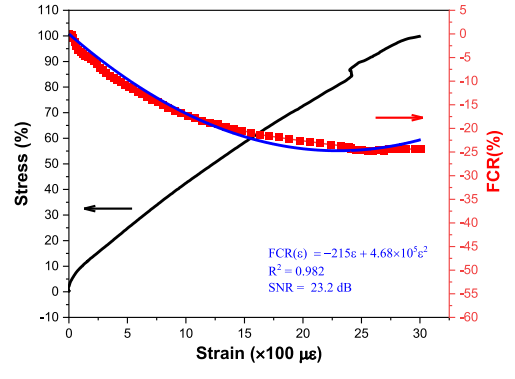

(g) 20CB02CNF

Fig. 20. Piezoresistive sensing performance for all groups under monotonic compressive loading.

3.5.3. Monotonic compressive loading

Fig. 20 presents piezoresistive sensing behaviour of all groups under monotonic compressive loading. It is seen that the sensitivity generally shows a consistent trend with the counterparts under quasi-static cyclic loading and dynamic cyclic loading. According to previous studies [31, 97], the correlation between FCR and strain can be modeled as a quadratic polynomial form based on effective conductive path theory and tunnelling theory, which is expressed as Eq. (15):

$$\mathrm{FCR}\ (\varepsilon) = \mathrm{A}\varepsilon + \mathrm{B}\varepsilon^2 \tag{15}$$

where *A* and *B* are fitting coefficients.

Mathematic regression analysis is carried out on the experimental data of present study by Eq. (15). As shown in Fig. 20, fitting curves generally show a high degree coefficient of determination with the experimental data. The established correlations between FCR and strain can function as calibration curve for the cement-based sensors, thereby laying a theoretical foundation for application of strain monitoring in practical engineering [105]. In addition, the coefficient of determination (R^2) is always higher for hybrid CB/CNF filled samples compared to the counterpart for single CB filled samples regardless of the CB content, which indicate better sensing signal with less fluctuation. The enhanced sensing signal with less noise is further supported by the higher SNR values for hybrid CB/CNF filled samples than the counterparts for single CB filled samples regardless of the CB content. This should imply the synergetic enhancing effect for hybrid CNF/CB filled samples compared to single CB filled samples. Due to the granular shape of CB particles, the conductive network made up by CB alone may more easily disturbed during the monotonic compressive loading process. Fibrous CNF plays the essential role as long-range conductor and fills the gaps between granular CB to form a more stable and homogeneous conductive network. Overall, the results indicate the hybrid use of CNF can enhance the stability of piezoresistive sensing performance of single CB filled UHPC with less signal noise under the monotonic compressive loading.

4. Conclusions

The single CB and hybrid CB/CNF UHPC filled samples were compared in terms of the strength, microstructures, percolation threshold, conductivity and piezoresistive sensing performance in this study. Based on the experimental data, the electrical microstructure and conductive behaviour were analysed by ACIS and equivalent circuit model. The main conclusion and novel findings are summarized as follows.

(1) For both single CB and hybrid CB/CNF filled samples, the compressive strength slightly increases when CB content is 0.5 % and then remarkably decreases when CB contents reach the 1.0 % and 2.0 %. It is seen that hybrid CB/CNF filled samples always show the superior compressive strength than single CB filled samples, regardless of the CB content.

(2) The percolation zone for both types of UHPC start at approximately 0.5 % CB content. Compared to single filled UHPC samples, hybrid CB/CNF filled UHPC samples show the lower resistivity except for the case of 0.5 % CB, which is probably owing to refined porosity. The maximum extent of drop in resistivity happens in intermediate CB content of 1.0 %.

(3) Microstructural analysis reveals the tight bonding between CNF and surrounding CB/hydration products in UHPC samples, which should be beneficial to the formation of continuous passages. EDS mapping spectrum clearly demonstrates the role of CNF that links the surrounding conductive passages contributed by CB nanoparticles, evidencing the cooperative modification effect brought by the hybrid usage of nanoaddtives with different sizes and dimensions.

(4) Based on experimental results and conductive phases involved in microstructures, a novel equivalent circuit model ($(R_1(C_1R_2))(R_3Q)(R_4W)$) is proposed to characterize the electrical conductive behaviours for both single CB and hybrid CB/CNF filled UHPC samples. The essential information concerning conductive behaviours can be properly extracted from a semi-qualitative point of view, based on the variations of equivalent circuit parameters that are assigned to different electrical phases involved in the microstructures. The obtained essential information such as the percolating state of CB and the different forms of how CNF contribute to conductive network in hybrid CB/CNF filled UHPC can help understand the conductive behaviours and working mechanisms at microstructural level.

(5) Under quasi-static cyclic loading, both the single CB and hybrid CB/CNF filled composites show the competent stress and strain – sensing capacities. The piezoresistive sensitivity of 05CB02CNF is comparable to 05CB. Differently, 10CB02CNF shows a distinctive higher sensitivity than 10CB while 20CB02CNF shows a reduced sensitivity than 20CB. The variation trend of sensitivities for the piezoresistive responses of hybrid CB/CNF filled UHPC compared to single CB filled UHPC shows a good coincidence with conductive behaviours extracted from the analysis of percolation threshold, electrical microstructure, and equivalent electrical circuit.

(6) Under dynamic load, the variation of piezoresistive sensitivities for different groups are generally consistent with the counterparts under quasi-static load. The stability of piezoresistive sensing performance in response to dynamic cyclic load improves with increasing content of conductive fillers. The hybrid use of CNF can enhance the stability of piezoresistive sensing performance of single CB filled UHPC with less signal noise under the monotonic compressive loading.

CRediT authorship contribution statement

Wengui Li: Writing – review & editing, Writing – original draft, Supervision, Resources, Methodology, Funding acquisition, Conceptualization. **Yipu Guo:** Writing – review & editing, Writing – original draft, Validation, Methodology, Investigation, Data curation. **Xuanrui Zhang:** Writing – review & editing, Writing – original draft. **Wenkui Dong:** Writing – review & editing, Writing – original draft. **Xiaohu Li:** Investigation, Visualization, Writing – original draft, Writing – review & editing. **Tao Yu:** Writing – review & editing, Writing – original draft. **Kejin Wang:** Writing – review & editing, Writing – original draft, Validation, Supervision, Formal analysis.

Declaration of competing interest

The authors declare that they have no known competing financial interests or personal relationships that could have appeared to influence the work reported in this paper.

Data availability

Data will be made available on request.

Acknowledgements

The authors appreciate the support of Australian Research Council (ARC), Australia (FT220100177, LP230100288, DP220101051, DP220100036; IH200100010). The second author (Yipu Guo) also thanks the China Scholarship Council (CSC).

References

[1] C.D. Atkinson, F. Aslani, Performance of 3D printed columns using self-sensing cementitious composites, Construct. Build. Mater. 375 (2023) 130961.
[2] W. Dong, W. Li, Y. Guo, X. He, D. Sheng, Effects of silica fume on physicochemical properties and piezoresistivity of intelligent carbon black-cementitious composites, Construct. Build. Mater. 259 (2020) 120399.
[3] E. García-Macías, F. Ubertini, Real-time Bayesian damage identification enabled by sparse PCE-Kriging meta-modelling for continuous SHM of large-scale civil engineering structures, J. Build. Eng. 59 (2022) 105004.
[4] G. Yıldırım, O. Öztürk, A. Al-Dahawi, A.A. Ulu, M. Şahmaran, Self-sensing capability of engineered cementitious composites: effects of aging and loading conditions, Construct. Build. Mater. 231 (2020) 117132.
[5] W. Dong, W. Li, Z. Tao, K. Wang, Piezoresistive properties of cement-based sensors: review and perspective, Construct. Build. Mater. 203 (2019) 146–163.
[6] E. García-Macías, A. D'Alessandro, R. Castro-Triguero, D. Perez-Mira, F. Ubertini, Micromechanics modeling of the uniaxial strain-sensing property of carbon nanotube cement-matrix composites for SHM applications, Compos. Struct. 163 (2017) 195–215.
[7] W. Dong, W. Li, X. Zhu, D. Sheng, S.P. Shah, Multifunctional cementitious composites with integrated self-sensing and hydrophobic capacities toward smart structural health monitoring, Cement Concr. Compos. 118 (2021) 103962.
[8] S.-J. Lee, I. You, S. Kim, H.-O. Shin, D.-Y. Yoo, Self-sensing capacity of ultra-high-performance fiber-reinforced concrete containing conductive powders in tension, Cement Concr. Compos. 125 (2022) 104331.
[9] Y. Li, T. Mi, W. Liu, Z. Dong, B. Dong, L. Tang, F. Xing, Chemical and mineralogical characteristics of carbonated and uncarbonated cement pastes subjected to high temperatures, Compos. B Eng. 216 (2021) 108861.
[10] Z. Chen, J.L.G. Lim, E.-H. Yang, Ultra high performance cement-based composites incorporating low dosage of plasma synthesized carbon nanotubes, Mater. Des. 108 (2016) 479–487.
[11] J. Seo, D. Jang, B. Yang, H.N. Yoon, J.G. Jang, S. Park, H.-K. Lee, Material characterization and piezoresistive sensing capability assessment of thin-walled CNT-embedded ultra-high performance concrete, Cement Concr. Compos. 134 (2022) 104808.
[12] M. Jung, Y.-s. Lee, S.-G. Hong, J. Moon, Carbon nanotubes (CNTs) in ultra-high performance concrete (UHPC): dispersion, mechanical properties, and electromagnetic interference (EMI) shielding effectiveness (SE), Cement Concr. Res. 131 (2020) 106017.
[13] M. Jung, J. Park, S.-g. Hong, J. Moon, Electrically cured ultra-high performance concrete (UHPC) embedded with carbon nanotubes for field casting and crack sensing, Mater. Des. 196 (2020) 109127.
[14] L. Guo, J. Wu, H. Wang, Mechanical and perceptual characterization of ultra-high-performance cement-based composites with silane-treated graphene nano-platelets, Construct. Build. Mater. 240 (2020) 117926.
[15] H. Wang, X. Gao, J. Liu, M. Ren, A. Lu, Multi-functional properties of carbon nanofiber reinforced reactive powder concrete, Construct. Build. Mater. 187 (2018) 699–707.
[16] S. Wen, D. Chung, Partial replacement of carbon fiber by carbon black in multifunctional cement–matrix composites, Carbon 45 (3) (2007) 505–513.
[17] B. Han, L. Zhang, S. Sun, X. Yu, X. Dong, T. Wu, J. Ou, Electrostatic self-assembled carbon nanotube/nano carbon black composite fillers reinforced cement-based materials with multifunctionality, Compos. Appl. Sci. Manuf. 79 (2015) 103–115.
[18] L. Liu, J. Xu, T. Yin, Y. Wang, H. Chu, Improving electrical and piezoresistive properties of cement-based composites by combined addition of nano carbon black and nickel nanofiber, J. Build. Eng. 51 (2022) 104312.
[19] L. Zhang, B. Han, J. Ouyang, X. Yu, S. Sun, J. Ou, Multifunctionality of cement based composite with electrostatic self-assembled CNT/NCB composite filler, Arch. Civ. Mech. Eng. 17 (2) (2017) 354–364.
[20] L. Zhang, S. Ding, L. Li, S. Dong, D. Wang, X. Yu, B. Han, Effect of characteristics of assembly unit of CNT/NCB composite fillers on properties of smart cement-based materials, Compos. Appl. Sci. Manuf. 109 (2018) 303–320.
[21] S. Ding, Y. Ruan, X. Yu, B. Han, Y.-Q. Ni, Self-monitoring of smart concrete column incorporating CNT/NCB composite fillers modified cementitious sensors, Construct. Build. Mater. 201 (2019) 127–137.
[22] L. Qiu, S. Ding, D. Wang, B. Han, Self-sensing GFRP-reinforced concrete beams containing carbon nanotube-nano carbon black composite fillers, Meas. Sci. Technol. 34 (8) (2023) 084003.
[23] H. Zhao, Y. Hu, Y. Li, K. Wang, F. Dehn, W. Li, Triaxial compressive performance of recycled aggregate/glass sand concrete: Experimental study and mechanism analysis, J. Clean. Prod. 442 (2024) 141006.
[24] K. Chen, Q. Liu, B. Chen, S. Zhang, L. Ferrara, Effect of raw materials on the performance of 3D printing geopolymer: A review, J. Build. Eng. 84 (2024) 108501.
[25] C. Astm, Standard Test Method for Flow of Hydraulic Cement Mortar, 2007, p. C1437.
[26] Y. Guo, W. Li, W. Dong, Z. Luo, F. Qu, F. Yang, K. Wang, Self-sensing performance of cement-based sensor with carbon black and polypropylene fibre subjected to different loading conditions, J. Build. Eng. 59 (2022) 105003.
[27] Y.-y. Hou, M.-q. Sun, J.-z. Chen, Electrical resistance and capacitance responses of smart ultra-high performance concrete with compressive strain by DC and AC measurements, Construct. Build. Mater. 327 (2022) 127007.
[28] R. Wang, F. He, C. Shi, D. Zhang, C. Chen, L. Dai, AC impedance spectroscopy of cement-based materials: measurement and interpretation, Cement Concr. Compos. 131 (2022) 104591.
[29] G. Hsieh, S. Ford, T. Mason, L. Pederson, Experimental limitations in impedance spectroscopy: Part I—simulation of reference electrode artifacts in three-point measurements, Solid State Ionics 91 (3–4) (1996) 191–201.
[30] A.L. Materazzi, F. Ubertini, A. D'Alessandro, Carbon nanotube cement-based transducers for dynamic sensing of strain, Cement Concr. Compos. 37 (2013) 2–11.
[31] Y. Suo, H. Xia, R. Guo, Y. Yang, Study on self-sensing capabilities of smart cements filled with graphene oxide under dynamic cyclic loading, J. Build. Eng. 58 (2022) 104775.
[32] Q. Zhang, C. Luan, C. Yu, Y. Huang, Z. Zhou, Mechanisms of carbon black in multifunctional cement matrix: hydration and microstructure perspectives, Construct. Build. Mater. 346 (2022) 128455.
[33] A. Fehervari, A.J.N. MacLeod, E.O. Garcez, L. Aldridge, W.P. Gates, Y. Yang, F. Collins, On the mechanisms for improved strengths of carbon nanofiber-enriched mortars, Cement Concr. Res. 136 (2020) 106178.
[34] C.-M. Aldea, F. Young, K. Wang, S.P. Shah, Effects of curing conditions on properties of concrete using slag replacement, Cement Concr. Res. 30 (3) (2000) 465–472.
[35] M.R. Irshidat, N. Al-Nuaimi, W. Ahmed, M. Rabie, Feasibility of recycling waste carbon black in cement mortar production: environmental life cycle assessment and performance evaluation, Construct. Build. Mater. 296 (2021) 123740.
[36] W. Dong, W. Li, L. Shen, D. Sheng, Piezoresistive behaviours of carbon black cement-based sensors with layer-distributed conductive rubber fibres, Mater. Des. 182 (2019) 108012.
[37] C.S. Karadumpa, R.K. Pancharathi, Influence of particle packing theories on strength and microstructure properties of composite cement–based mortars, J. Mater. Civ. Eng. 33 (10) (2021) 04021267.
[38] L. Li, B. Wang, M.H. Hubler, Carbon nanofibers (CNFs) dispersed in ultra-high performance concrete (UHPC): mechanical property, workability and permeability investigation, Cement Concr. Compos. 131 (2022) 104592.
[39] W. Dong, W. Li, N. Lu, F. Qu, K. Vessalas, D. Sheng, Piezoresistive behaviours of cement-based sensor with carbon black subjected to various temperature and water content, Compos. B Eng. 178 (2019) 107488.
[40] T. Wang, J. Xu, B. Meng, G. Peng, Experimental study on the effect of carbon nanofiber content on the durability of concrete, Construct. Build. Mater. 250 (2020) 118891.
[41] Y. Gao, X. Zhu, D.J. Corr, M.S. Konsta-Gdoutos, S.P. Shah, Characterization of the interfacial transition zone of CNF-Reinforced cementitious composites, Cement Concr. Compos. 99 (2019) 130–139.
[42] F. Sanchez, C. Ince, Microstructure and macroscopic properties of hybrid carbon nanofiber/silica fume cement composites, Compos. Sci. Technol. 69 (7–8) (2009) 1310–1318.
[43] A. Standard, Standard Practice for Fabricating and Testing Specimens of Ultra-high Performance Concrete, ASTM International, West Conshohocken, PA, 2017.
[44] X. Li, H. Deng, Q. Zhang, F. Chen, Q. Fu, The effect of DBP of carbon black on the dynamic self-assembly in a polymer melt, RSC Adv. 6 (30) (2016) 24843–24852.
[45] G.H. Nalon, J.C.L. Ribeiro, E.N.D. de Araújo, L.G. Pedroti, J.M.F. de Carvalho, R. F. Santos, A. Aparecido-Ferreira, Effects of different kinds of carbon black nanoparticles on the piezoresistive and mechanical properties of cement-based composites, J. Build. Eng. 32 (2020) 101724.
[46] A.O. Monteiro, P.B. Cachim, P.M. Costa, Self-sensing piezoresistive cement composite loaded with carbon black particles, Cement Concr. Compos. 81 (2017) 59–65.
[47] S. Dong, L. Li, A. Ashour, X. Dong, B. Han, Self-assembled 0D/2D nano carbon materials engineered smart and multifunctional cement-based composites, Construct. Build. Mater. 272 (2021) 121632.
[48] G. Xu, J. Beaudoin, C. Jolicoeur, M. Pagé, Interfacial transition zone characterization of Portland cement mortars containing relatively high dosages of polynaphthalene sulfonate superplasticizers, Concrete Science and Engineering (France) 2 (7) (2000) 150–157.
[49] G. Xu, J. Beaudoin, C. Jolicoeur, M. Pagé, The effect of a polynaphthalene sulfonate superplasticizer on the contribution of the interfacial transition zone to the electrical resistivity of mortars containing silica and limestone fine aggregate, Cement Concr. Res. 30 (5) (2000) 683–691.
[50] X. Long, M. Sun, Z. Li, X. Song, Piezo-resistive effects in carbon black-filled cement-matrix nanocomposites, J. Wuhan Univ. Technol. 3 (2008) 57–59.
[51] Y. Dai, M. Sun, C. Liu, Z. Li, Electromagnetic wave absorbing characteristics of carbon black cement-based composites, Cement Concr. Compos. 32 (7) (2010) 508–513.
[52] A. Hussain, Y. Xiang, T. Yu, F. Zou, Nanocarbon black-based ultra-high-performance concrete (UHPC) with self-strain sensing capability, Construct. Build. Mater. 359 (2022) 129496.
[53] L. Wang, F. Aslani, Development of self-sensing cementitious composites incorporating CNF and hybrid CNF/CF, Construct. Build. Mater. 273 (2021) 121659.
[54] P. Hewlett, M. Liska, Lea's Chemistry of Cement and Concrete, Butterworth-Heinemann, 2019.
[55] Y.-W. Chan, S.-H. Chu, Effect of silica fume on steel fiber bond characteristics in reactive powder concrete, Cement Concr. Res. 34 (7) (2004) 1167–1172.
[56] S.H. Lee, S. Kim, D.-Y. Yoo, Hybrid effects of steel fiber and carbon nanotube on self-sensing capability of ultra-high-performance concrete, Construct. Build. Mater. 185 (2018) 530–544.
[57] Z. Luo, W. Li, K. Wang, A. Castel, S.P. Shah, Comparison on the properties of ITZs in fly ash-based geopolymer and Portland cement concretes with equivalent flowability, Cement Concr. Res. 143 (2021) 106392.

[58] A.A. Elseady, I. Lee, Y. Zhuge, X. Ma, C.W. Chow, N. Gorjian, Piezoresistivity and AC impedance spectroscopy of cement-based sensors: basic concepts, Interpretation, and Perspective, Materials 16 (2) (2023) 768.

[59] W. Pichor, M. Frąc, M. Radecka, Determination of percolation threshold in cement composites with expanded graphite by impedance spectroscopy, Cement Concr. Compos. 125 (2022) 104328.

[60] C.G. Berrocal, K. Hornbostel, M.R. Geiker, I. Löfgren, K. Lundgren, D.G. Bekas, Electrical resistivity measurements in steel fibre reinforced cementitious materials, Cement Concr. Compos. 89 (2018) 216–229.

[61] H.V. Le, M.K. Kim, D.J. Kim, J. Park, Electrical properties of smart ultra-high performance concrete under various temperatures, humidities, and age of concrete, Cement Concr. Compos. 118 (2021) 103979.

[62] N. Lee, S. Kim, G. Park, The effects of multi-walled carbon nanotubes and steel fibers on the AC impedance and electromagnetic shielding effectiveness of high-performance, fiber-reinforced cementitious composites, Materials 12 (21) (2019) 3591.

[63] J. Torrents, T. Mason, E. Garboczi, Impedance spectra of fiber-reinforced cement-based composites: a modeling approach, Cement Concr. Res. 30 (4) (2000) 585–592.

[64] H.V. Le, D.H. Lee, D.J. Kim, Effects of steel slag aggregate size and content on piezoresistive responses of smart ultra-high-performance fiber-reinforced concretes, Sensor Actuator Phys. 305 (2020) 111925.

[65] S. Wansom, N. Kidner, L. Woo, T. Mason, AC-impedance response of multi-walled carbon nanotube/cement composites, Cement Concr. Compos. 28 (6) (2006) 509–519.

[66] X. Li, M. Li, Multifunctional self-sensing and ductile cementitious materials, Cement Concr. Res. 123 (2019) 105714.

[67] G. Song, Equivalent circuit model for AC electrochemical impedance spectroscopy of concrete, Cement Concr. Res. 30 (11) (2000) 1723–1730.

[68] Y.J. Wang, Y. Pan, X.W. Zhang, K. Tan, Impedance spectra of carbon black filled high-density polyethylene composites, J. Appl. Polym. Sci. 98 (3) (2005) 1344–1350.

[69] J. Han, J. Cai, J. Pan, Y. Sun, Study on the conductivity of carbon fiber self-sensing high ductility cementitious composite, J. Build. Eng. 43 (2021) 103125.

[70] L. Jiang, Z. Liu, Y. Yu, X. Ben, The effect of graphene on the conductivity of magnesium sulfate cement, Construct. Build. Mater. 312 (2021) 125342.

[71] H. Allam, F. Duplan, S. Amziane, Y. Burtschell, Assessment of manufacturing process efficiency in the dispersion of carbon fibers in smart concrete by measuring AC impedance, Cement Concr. Compos. 127 (2022) 104394.

[72] L. Zhang, S. Ding, B. Han, X. Yu, Y.-Q. Ni, Effect of water content on the piezoresistive property of smart cement-based materials with carbon nanotube/nanocarbon black composite filler, Compos. Appl. Sci. Manuf. 119 (2019) 8–20.

[73] D.A. Triana-Camacho, D.A. Miranda, E. García-Macías, O.A.M. Reales, J. H. Quintero-Orozco, Effective medium electrical response model of carbon nanotubes cement-based composites, Construct. Build. Mater. 344 (2022) 128293.

[74] J. Xu, W. Zhong, W. Yao, Modeling of conductivity in carbon fiber-reinforced cement-based composite, J. Mater. Sci. 45 (2010) 3538–3546.

[75] B. Han, S. Ding, X. Yu, Intrinsic self-sensing concrete and structures: a review, Measurement 59 (2015) 110–128.

[76] G. Li, L. Wang, C. Leung, R. Hu, X. Zhao, B. Yan, J. Zhou, Effect of styrene-butadiene rubber on the electrical properties of carbon black/cement mortar, RSC Adv. 5 (86) (2015) 70229–70237.

[77] E. García-Macías, A. Downey, A. D'Alessandro, R. Castro-Triguero, S. Laflamme, F. Ubertini, Enhanced lumped circuit model for smart nanocomposite cement-based sensors under dynamic compressive loading conditions, Sensor Actuator Phys. 260 (2017) 45–57.

[78] B. Dong, Y. Wu, X. Teng, Z. Zhuang, Z. Gu, J. Zhang, F. Xing, S. Hong, Investigation of the Cl− migration behavior of cement materials blended with fly ash or/and slag via the electrochemical impedance spectroscopy method, Construct. Build. Mater. 211 (2019) 261–270.

[79] J. Han, J. Pan, J. Cai, X. Li, A review on carbon-based self-sensing cementitious composites, Construct. Build. Mater. 265 (2020) 120764.

[80] M. Cabeza, M. Keddam, X. Nóvoa, I. Sánchez, H. Takenouti, Impedance spectroscopy to characterize the pore structure during the hardening process of Portland cement paste, Electrochim. Acta 51 (8–9) (2006) 1831–1841.

[81] J. Cruz, I. Fita, L. Soriano, J. Payá, M. Borrachero, The use of electrical impedance spectroscopy for monitoring the hydration products of Portland cement mortars with high percentage of pozzolans, Cement Concr. Res. 50 (2013) 51–61.

[82] C. Song, S. Choi, Moisture-dependent piezoresistive responses of CNT-embedded cementitious composites, Compos. Struct. 170 (2017) 103–110.

[83] J. Zhang, A. Heath, H.M.T. Abdalgadir, R.J. Ball, K. Paine, Electrical impedance behaviour of carbon fibre reinforced cement-based sensors at different moisture contents, Construct. Build. Mater. 353 (2022) 129049.

[84] B. Dong, Q. Qiu, J. Xiang, C. Huang, H. Sun, F. Xing, W. Liu, Electrochemical impedance interpretation of the carbonation behavior for fly ash–slag–cement materials, Construct. Build. Mater. 93 (2015) 933–942.

[85] B. Dong, Q. Qiu, Z. Gu, J. Xiang, C. Huang, Y. Fang, F. Xing, W. Liu, Characterization of carbonation behavior of fly ash blended cement materials by the electrochemical impedance spectroscopy method, Cement Concr. Compos. 65 (2016) 118–127.

[86] W.-w. Li, W.-m. Ji, G.-h. Fang, Y.-q. Liu, F. Xing, Y.-k. Liu, B.-q. Dong, Electrochemical impedance interpretation for the fracture toughness of carbon nanotube/cement composites, Construct. Build. Mater. 114 (2016) 499–505.

[87] B. Díaz, B. Guitián, X.R. Nóvoa, C. Pérez, Conductivity assessment of multifunctional cement pastes by impedance spectroscopy, Corrosion Sci. 185 (2021) 109441.

[88] L. Wang, F. Aslani, A review on material design, performance, and practical application of electrically conductive cementitious composites, Construct. Build. Mater. 229 (2019) 116892.

[89] B. Díaz, B. Guitián, X. Nóvoa, C. Pérez, Analysis of the microstructure of carbon fibre reinforced cement pastes by impedance spectroscopy, Construct. Build. Mater. 243 (2020) 118207.

[90] L. Zhang, L. Li, Y. Wang, X. Yu, B. Han, Multifunctional cement-based materials modified with electrostatic self-assembled CNT/TiO2 composite filler, Construct. Build. Mater. 238 (2020) 117787.

[91] P.A. Danoglidis, M.S. Konsta-Gdoutos, S.P. Shah, Relationship between the carbon nanotube dispersion state, electrochemical impedance and capacitance and mechanical properties of percolative nanoreinforced OPC mortars, Carbon 145 (2019) 218–228.

[92] W. Hsu, V. Kotzeva, P. Watts, G. Chen, Circuit elements in carbon nanotube-polymer composites, Carbon 42 (8–9) (2004) 1707–1712.

[93] D.E. Macphee, D.C. Sinclair, S.L. Cormack, Development of an equivalent circuit model for cement pastes from microstructural considerations, J. Am. Ceram. Soc. 80 (11) (1997) 2876–2884.

[94] X. Hu, C. Shi, X. Liu, J. Zhang, G. De Schutter, A review on microstructural characterization of cement-based materials by AC impedance spectroscopy, Cement Concr. Compos. 100 (2019) 1–14.

[95] D. Vladikova, The technique of the differential impedance analysis part I: basics of the impedance spectroscopy, in: Proceedings of the International Workshop on Advanced Techniques for Energy Sources Investigation and Testing, 2004, pp. 1–28.

[96] M. Cabeza, P. Merino, A. Miranda, X. Nóvoa, I. Sanchez, Impedance spectroscopy study of hardened Portland cement paste, Cement Concr. Res. 32 (6) (2002) 881–891.

[97] L. Qiu, S. Dong, X. Yu, B. Han, Self-sensing ultra-high performance concrete for in-situ monitoring, Sensor Actuator Phys. 331 (2021) 113049.

[98] S. Ding, S. Dong, A. Ashour, B. Han, Development of sensing concrete: principles, properties and its applications, J. Appl. Phys. 126 (24) (2019) 241101.

[99] H. Xiao, H. Li, J. Ou, Modeling of piezoresistivity of carbon black filled cement-based composites under multi-axial strain, Sensor Actuator Phys. 160 (1–2) (2010) 87–93.

[100] J.G. Simmons, Generalized formula for the electric tunnel effect between similar electrodes separated by a thin insulating film, J. Appl. Phys. 34 (6) (1963) 1793–1803.

[101] I. You, D.-Y. Yoo, S. Kim, M.-J. Kim, G. Zi, Electrical and self-sensing properties of ultra-high-performance fiber-reinforced concrete with carbon nanotubes, Sensors 17 (11) (2017) 2481.

[102] D.-Y. Yoo, S. Kim, S.H. Lee, Self-sensing capability of ultra-high-performance concrete containing steel fibers and carbon nanotubes under tension, Sensor Actuator Phys. 276 (2018) 125–136.

[103] F. Song, Q. Chen, M. Zhang, Z. Jiang, W. Ding, Z. Yan, H. Zhu, Exploring the piezoresistive sensing behaviour of ultra-high performance concrete: strategies for multiphase and multiscale functional additives and influence of electrical percolation, Compos. B Eng. (2023) 111042.

[104] A. Monteiro, P. Costa, M. Oeser, P. Cachim, Dynamic sensing properties of a multifunctional cement composite with carbon black for traffic monitoring, Smart Mater. Struct. 29 (2) (2020) 025023.

[105] Y. Jiang, J. Xu, Z. Yu, L. Liu, H. Chu, Improving conductivity and self-sensing properties of magnetically aligned electroless nickel coated glass fiber cement, Cement Concr. Compos. (2023) 104929.